Contrib Mineral Petrol (1981) 77:337–354

Contributions to Mineralogy and Petrology

Petrology and Geochemistry of the Island of Sarigan in the Mariana Arc; Calc-Alkaline Volcanism in an Oceanic Setting

Arend Meijer and Mark Reagan
Department of Geosciences, University of Arizona, Tucson, Arizona 85721, USA

Abstract. Isotopic studies of rocks from oceanic island arcs such as the Marianas indicate that little, if any, recycling of continental material (e.g. oceanic sediments) occurs in these arcs. Because oceanic arcs are on the average more mafic than the dominantly andesitic continental arcs, an important question is whether the andesites of continental arcs are produced by a fundamentally different (more complex?) mechanism than the lavas of oceanic arcs. An excellent opportunity for study of this question is provided by the island of Sarigan, in the Mariana active arc, on which calc-alkaline andesites (including hornblende-bearing types) are exposed along with more mafic lavas.

Available isotope data suggest the Sarigan lavas (including the andesites) were derived from mantle material with little or no involvement of continental components. Ratios of incompatible elements suggest that most of the Sarigan lavas were derived from similar source materials. Absolute abundances of incompatible elements vary irregularly within the eruptive sequence and indicate at least 5 distinct magma batches are represented on Sarigan.

Major element data obtained on the lavas and mineral phases in them, combined with modal mineral abundances, suggest that the calc-alkaline nature of the volcanic rocks on Sarigan results from the fractional crystallization of titanomagnetite in combination with other anhydrous phases. Amphibole, although present in some samples, is mainly a late-crystallizing phase and did not produce the calc-alkline characteristics of these lavas. Gabbroic samples found in the volcanic sequence have mineralogic and geochemical characteristics that would be expected of residual solids produced during fractional crystallization of the Sarigan lavas. When combined, data on the lavas and the gabbros suggest the following crystallization sequence: olivine – plagioclase – clinopyroxene – titanomagnetite – orthopyroxene ± hornblende, biotite and accessory phases.

These results lead to the conclusion that calc-alkaline magmas can be generated directly from mantle sources.

Introduction

Studies of the origin (i.e. source materials) of calc-alkaline andesites from continental arcs have been hampered by uncertainty concerning the degree to which magmas derived from below the crust may have been "contaminated" by reaction with the crust during ascent. This is particularly evident in the isotopic studies (e.g. Ewart and Stipp 1968; Armstrong and Cooper 1971; Church 1976). To sidestep this uncertainty, isotopic studies have been carried out on lavas from oceanic arcs well away from continental areas (e.g. Sinha and Hart 1972; Oversby and Ewart 1972; Meijer 1976; Kay et al. 1978; Hawkesworth et al. 1979). These studies have generally found little, if any, evidence for the involvement of continental material in the genesis of lavas erupted in these arcs. The question remains as to what implications these results have for the genesis of magmas in continental arcs.

According to recent reviews (Miyashiro 1974; Ewart 1976), lavas erupted in continental and oceanic arcs show some consistent differences. Oceanic arc lavas generally have lower alkali and SiO_2 contents, more pronounced Fe enrichment trends, a greater proportion of basalts and basaltic andesites and they less commonly contain hydrous phases. The important question in the present context is whether these differences reflect distinct origins for continental and oceanic arc lavas or simply variations on the same basic magma generation process.

We have studied a sequence of lavas on the island of Sarigan in the Mariana arc which bears on this question. The lavas of this sequence have many of the characteristics attributed to lavas erupted in continental arcs even though they were clearly erupted in an oceanic arc. The results of our studies should help bridge the gap in our understanding of the origin of oceanic and continental arc lavas.

Regional Setting

Sarigan Island is part of the active volcanic arc associated with the Mariana arc system (Karig 1971). Subaerially, the arc stretches 500 km from Anatahan to Uracas (Fig. 1). Arc-related seamounts (Stern and Bibee 1980) extend this trend north of Uracas and south of Anatahan to a total length of 1,000 km. A striking feature of this arc is its near perfect curvature, clearly lacking the segmentation noted in other circum-Pacific arcs (Carr 1976; Marsh 1979).

Most of the subaerial cones and several of the seamounts are known to have been active within this century (Kuno 1962; Meijer 1981). Sarigan and Anatahan appear to be exceptions although they have undoubtedly been active in the last 10,000 years judging from the sparse vegetation on the most recent flows.

Although the crustal thickness in the central part of the arc is not well defined (La Traille and Hussong 1980), the crust is clearly of oceanic character. Recent seismic studies suggest the active arc volcanoes are in part superimposed on the young (0–8 m.y.b.p.; Hussong and Uyeda et al. 1981) inter-arc basin crust of the Mariana Trough (Bibee et al. 1980). The crustal

0010-7999/81/0077/0337/$03.60

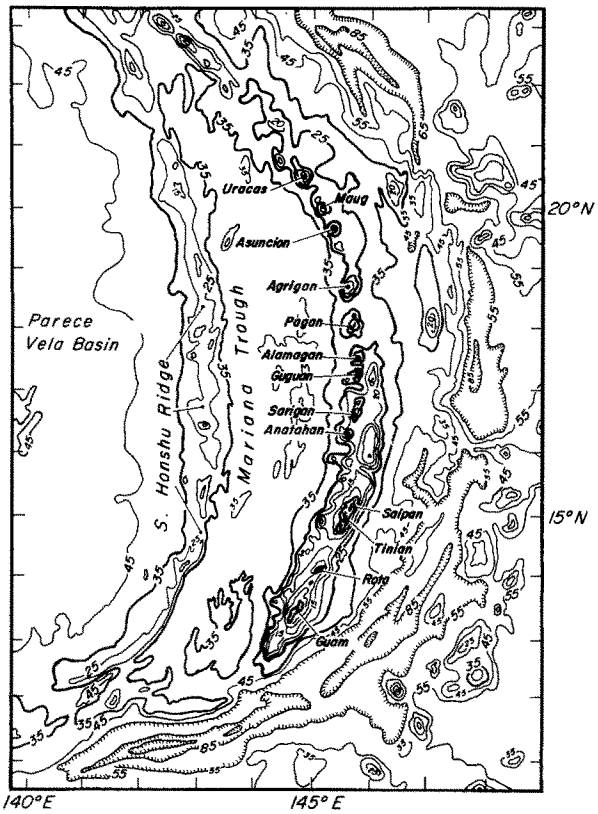

Fig. 1. Generalized bathymetric map of Mariana island arc system. Depth in thousands of meters (after Karig 1971)

section between the Mariana Trough and the Mariana Trench is composed of Eocene to Miocene arc rocks and younger sediments (Cloud et al. 1956; Tracey et al. 1963; Hussong and Uyeda et al. 1981).

Pacific lithosphere of Jurassic to Cretaceous age (Larson and Chase 1972) is being subducted westward beneath the arc system at a rate of approximately 4.0 cm/year (Seno 1977). Directly beneath the arc, the Benioff zone occurs at approximately 100 km, whereas at greater depths (i.e. beneath the Mariana Trough) the zone is essentially vertical (Katsumatu and Sykes 1969).

Sarigan Geology

The island of Sarigan is 3.1 km^2 in area and has a maximum elevation of 538 m. It represents the subaerial portion of a cone that is 1.8 km in total height, with a basal diameter of approximately 15 km. In the following, we shall deal only with the subaerial part of the Sarigan volcano.

The exact age of the sequence exposed on Sarigan is not well known. A sample of hornblende andesite from the upper portion of the sequence has been dated at 0.5 ± 0.2 m.y. by K-Ar methods (Meijer et al., unpublished). This result combined with the morphologic youthfulness of the *subaerial* cone suggests it is probably less than 1.0 m.y. old.

Morphologically, Sarigan is a low truncated cone with a small but well defined crater 0.75 km in diameter (Fig. 2). The lower slopes of the cone are buttressed by flow sequences at or near sea level while the upper slopes are generally blanketed by pyroclastic units covered by dense vegetation. The crater floor is nearly flat except for a small intra-crater ash cone along

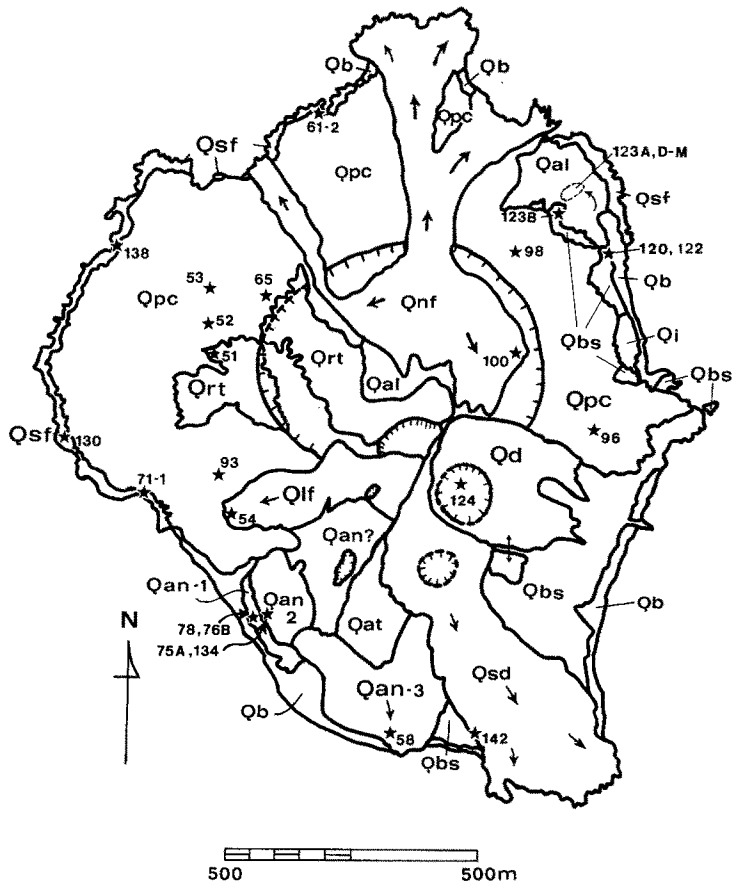

Fig. 2. Geologic map of Sarigan Island. Crater rim dashed where inferred. Note small craters on top of domes Qd and Qsd. Small ash cone shown in southern portion of main crater. *Arrows* on flows indicate flow directions. Sample localities shown as *stars*

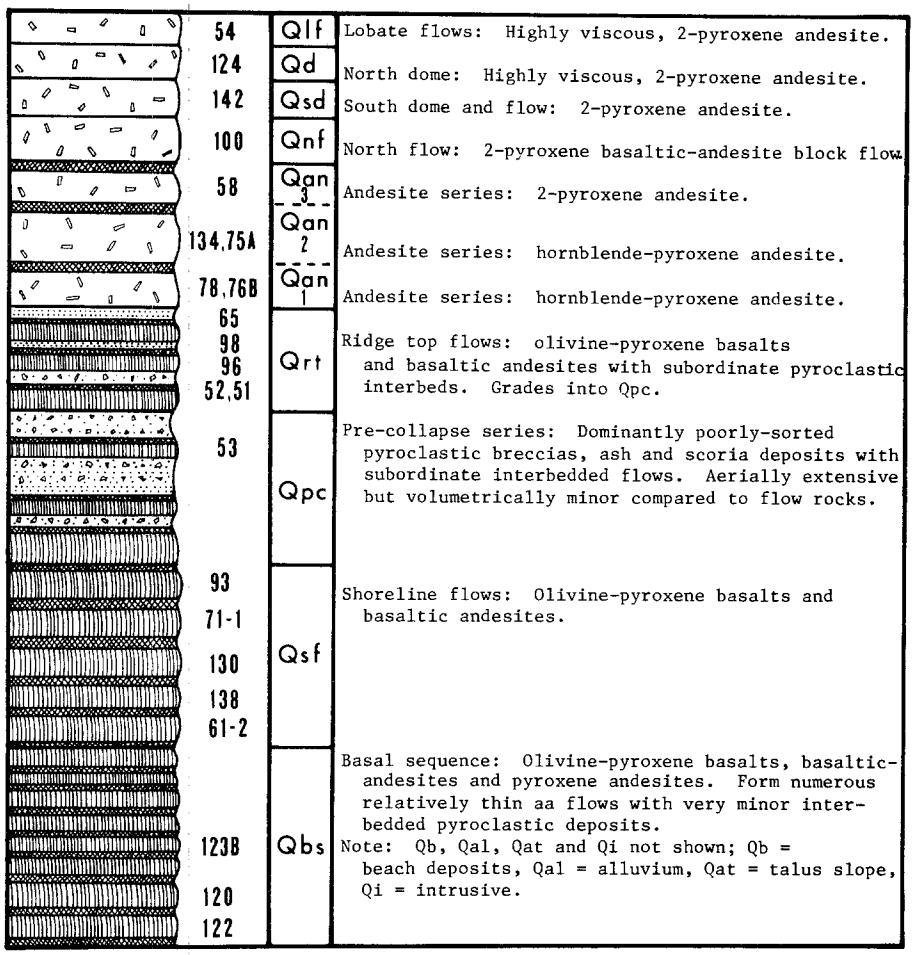

Fig. 3. Stratigraphy of Sarigan Island. Relative thicknesses approximate. Composite of several stratigraphic sections around island

the southern rim. The highest points on the island are formed by 2 domes of 2-pyroxene andesite intruded into the crater rim.

Volcanic Stratigraphy

The stratigraphic succession on Sarigan has been worked out on the basis of flow surface morphology (for the younger flows), superposition relations and correlation of widespread pyroclastic units. Correlation on the basis of geochemical criteria has been purposefully avoided so that the geochemical evolution could be independently established. The volcanic stratigraphy will be discussed below in terms of the volcanic events that formed the island (Fig. 3).

Subaerial volcanic activity was initiated with the eruption in rapid succession of a large number of thin (1–3 m) aa flows of basaltic andesite and andesite (Qbs; Fig. 2). This basal flow sequence is on the order of 250 m thick and contains less than 15% pyroclastic material. The flows generally consist of a dense or slightly vesicular core (30–50% by volume) sandwiched between upper and lower aa rubble zones (50–70%). The rapidity of eruption is suggested by the lack of paleosols in the flow sequence and the fact that the aa flow tops were not eroded between eruptions. A plug (18×20 m) of highly viscous lava was extruded laterally near the base of the cone on the northeast side, some time during this eruption sequence (Qi) as the plug is draped by the younger flows in the sequence. Excellent exposures of the sequence occur along the east coast of the island.

Eruption of the basal flow sequence was followed by a period of inactivity during which wave action eroded the lower slopes of the new cone. Activity resumed with the eruption of voluminous flows of basalt and basaltic andesite. These flows currently form the shorelines around much of the northern half of the island (Qsf, Fig. 2). Because they are more massive and occasionally have pahoe-hoe flow surfaces, these flows were probably hotter on eruption than the earlier flows. Their total thickness varies from 50 to 75 m with the greatest thicknesses at the shoreline.

A period of strong Strombolian activity followed the eruption of the shoreline flows and deposited a veneer (0.5–3 m) of scoria (not shown on Fig. 2) over most of the cone also filling a major valley in the southwestern sector. Overlying this unit is a heterogeneous sequence of volcanic breccias and ash 2–30 m in thickness. (Qpc; Fig. 2). The breccias contain rare gabbroic clasts mixed with a greater variety of volcanic rock fragments. Ash layers occur both above and below the breccias. It is likely these deposits were produced during the collapse event that resulted in the present crater. Small flows of viscous basaltic andesite issued from the crater during the latter part of this activity. Because they now form prominant ridges, these flows are designated the ridge top flows (Qrt).

A new ash cone formed inside the crater shortly after its formation. Eruptions from this cone deposited a thin (< 1.0 m) veneer of ash (not shown on Fig. 2) over much of the cone. These eruptions were followed by the extrusion of 3 andesite flows (2 bearing hornblende), each 15–20 m in thickness, from the southern rim of the crater (Qan; Fig. 2). Unlike other flows on the island, these flows show excellent columnar jointing and entablature.

Table 1. Modal composition of lavas (vol. %)

Unit	Qbf	Qbf	Qbf	Qsf	Qsf	Qsf	Qsf	Scoria	Qpc	Qpc
Sample no	SA-122	SA-120	SA-123B	SA-61-2	SA-138	SA130	SA-71-1	SA-93	SA-53	SA-52
Matrix	62.6	59.3	46.0	50.2	46.0	53.4	15.1	57.7	67.6	57.5
Pheno Plag[a]	21.3	19.8	23.4	14.1	26.8	24.3	22.3	25.5	19.3	23.5
Micro Plag[a]	1.1	4.8	10.0	10.8	5.6	7.5	26.4	3.5	1.8	5.3
Pheno cpx	9.5	5.2	12.3	17.9	15.0	5.6	17.1	10.5	5.1	10.0
Micro cpx	0.3	1.0	2.5	2.6	2.4	1.5	13.7	0.5	0.6	1.3
Pheno opx	2.5	7.7	3.0	2.4	2.5	6.3	1.0	0.5	4.0	1.0
Micro opx	0.0	0.9	0.3	0.5	0.2	1.3	0.2	0.0	0.0	0.1
Pheno Ol	0.7	0.1	0.6	0.2	0.3	0.0	1.2	0.4	0.0	0.1
Micro Ol	0.0	0.0	0.1	0.3	0.5	0.0	0.3	1.3	0.0	0.3
Pheno Fe–Ti[b]	1.7	0.6	0.4	0.1	0.2	0.3	0.0	0.16	0.3	0.4
Micro Fe–Ti[b]	0.3	0.7	1.4	0.9	0.5	2.5	2.6	0.0	0.65	0.5
Hemitite	0.0	0.0	0.0	0.0	0.0	0.0	0.1	0.0	0.0	0.0
Pheno Amph	0.0	0.0	0.0	0.0	0.0	0.0	0.0	0.0	0.0	0.0
Vesicles[c]	26.9	0.6	0.0	11.7	21.0	3.6	1.7	60.1	1.6	13.0
Pts Counted	1,368	1,058	1,086	1,132	1,266	1,011	1,043	2,509	1,049	1,164

[a] phenocrysts: ≥ 0.15 mm; microphenocrysts: 0.04–0.15 mm
[b] phenocrysts: >0.07 mm; microphenocrysts: 0.01–0.07 mm
[c] Vesicle % calculated independently of solid phases

The youngest activity produced a series of 2 flows and 2 domes of 2-pyroxene andesite that were extruded from the crater rim. The relative age relations among these units are not well established although they all appear to be of similar age based on surface morphology. The oldest unit was extruded as a flow from the northern rim of the crater (Qnf). It is similar to the shoreline flows (Qsf) in volume and form but has a blocky surface suggestive of lower eruption temperatures. The 3 younger units consist of a dome from which a viscous flow was extruded southeastward (Qsd) into the sea, a highly viscous flow which was extruded southwestward from a linear vent along the crater rim (Qlf) and a classic plug dome (Qnd).

The above discussion and other field observations suggest that (1) pyroclastics make up no more than 25 volume percent of the eruptive products now exposed, (2) the number and volume of pyroclastic eruptions increased through time, and (3) the viscosity of flows apparently increased through time following the eruption of the shoreline flows.

Petrography and Mineral Chemistry

The lavas of Sarigan typically have pilotaxitic textures and are generally highly porphyritic with phenocryst contents (Table 1) ranging from 30 to 50 volume percent (corrected for vesicle content). Pyroclastic materials of primary origin commonly have lower phenocryst abundances. Several size populations exist among the crystalline phases. In the following, a phenocryst is at least 0.15 mm in length while a microphenocryst is between 0.03 and 0.15 mm. Nearly all thin sections examined contain glomeroporphyritic clots, from 1 to 5 mm, of one or more of the minerals plagioclase, clinopyroxene, orthopyroxene, titanomagnetite and occasionally olivine. These clots have been interpreted by some as breakdown products of hornblende (Stewart 1975; Boettcher 1977). Clots resulting from the breakdown of hornblende do occur in some samples (Hornblende andesites) as evidenced by their relict amphibole crystal outlines. However, these clots have fine grained recrystallization textures unlike the irregularly shaped glomeroporphyritic clots which we interpret as primary crystal clots (see also Garcia and Jacobson 1979).

Gabbroic fragments collected from the breccia units generally have cumulate textures. Plagioclase and clinopyroxene are the dominant cumulus minerals while orthopyroxene, titanomagnetite, olivine, uralitic hornblende, apatite, minor glass and rare biotite comprise the inter-cumulus phases (Table 2). Glassy inclusions are found within crystals in most of the samples. In those lacking orthopyroxene and hydrous minerals, the inclusions contain only glass. Where orthopyroxene is also present (e.g. SA-123J), the inclusions contain glass plus minor vapor bubbles. Samples bearing hydrous minerals have inclusions containing glass, vapor bubbles and small daughter minerals (opaques $\pm$ silicates). These observations suggest the samples crystallized from magmas progressively more enriched in volatiles.

Plagioclase

In the lavas, plagioclase phenocrysts show a wide range of sizes, textures and compositions. Basically, 3 types of crystals can be distinguished: (1) anhedral to subhedral, inclusion-poor fragments of microphenocryst to phenocryst size with nearly unzoned An-rich cores and very thin (≤ 0.03 mm), more albitic rims, (2) subhedral to euhedral phenocrysts and microphenocrysts with abundant inclusions of glass $\pm$ pyroxene and titanomagnetite, and (3) subhedral to euhedral, inclusion-poor, highly zoned microphenocrysts and microlites.

Type (2) crystals can be subdivided into three groups on the bases of the size and distribution of their inclusions. These are: (2a) crystals with inclusion-rich cores surrounded by inclusion-free, highly zoned rims (see Dungan and Rhodes 1978; Fig. 5C–F), (2b) crystals with inclusion-rich cores surrounded progressively by a zoned inclusion-free rim, an unzoned inclusion-rich rim with smaller sized inclusion than the core and finally a highly zoned inclusion-free rim, and (2c) crystals with an inclusion-poor core enclosed in an unzoned inclusion-rich rim surrounded by a highly zoned inclusion-free rim. Following Lofgren (1974), Hibbard (1981) and others, we interpret the inclusions to be matrix glass and microlites trapped during rapid growth of the plagioclase crystals.

Several general correlations were observed between crystal

Table 1 (continued)

Qrt SA-51	Qrt SA-96	Qrt SA-98	Qrt SA-65	Qan 1 SA-78	Qan 1 SA-76B	Qan 2 SA-134	Qan 2 SA-75A	Qan 3 SA-58	Qnf SA-100	Qsd SA-142	Qd SA-124	Qlf SA-54
56.7	54.2	59.4	36.7	56.1	50.8	44.9	41.4	60.8	69.7	39.7	49.7	56.7
21.7	22.1	20.7	27.5	23.5	23.4	28.9	26.8	21.0	18.6	28.0	23.1	22.2
7.4	5.2	4.9	18.0	9.1	10.1	13.7	13.0	2.8	3.4	15.9	6.4	7.1
11.0	13.7	12.5	9.1	2.5	6.5	3.3	3.6	7.8	4.7	5.2	9.5	5.3
2.0	0.4	1.0	5.6	0.6	3.2	2.6	1.2	2.2	1.0	2.5	1.6	2.6
0.7	2.5	0.6	1.2	2.9	1.1	1.4	2.0	2.6	1.5	3.0	4.1	2.5
0.2	0.2	0.3	0.1	0.2	1.0	0.9	0.7	0.5	0.0	2.4	1.5	1.3
0.1	0.5	0.1	0.0	0.0	1.1	1.5	0.2	0.8	0.1	0.5	0.6	0.5
0.2	0.3	0.3	0.0	0.0	0.0	0.0	0.0	0.0	0.0	0.0	0.3	0.0
0.0	0.1	0.1	0.6	1.4	0.9	1.1	1.0	1.0	0.8	1.2	1.4	0.6
0.1	0.9	0.2	1.2	1.6	1.6	0.9	5.3	0.3	0.2	1.7	1.7	1.3
0.0	0.0	0.0	0.0	0.0	0.1	0.0	2.3	0.2	0.0	0.0	0.1	0.0
0.0	0.0	0.0	0.0	2.0	0.2	0.7	2.4	0.0	0.0	0.0	0.0	0.0
14.8	18.5	10.5	27.7	5.6	13.4	5.2	3.9	27.8	22.6	27.7	29.2	14.1
1,273	1,250	1,213	1,419	939	1,155	1,117	1,121	1,384	1,352	1,468	1,492	1,230

Table 2. Modal compositions of gabbros (vol. %)

Sample no.	Pts. Counted	Plag	Cpx	Oxide	Opx	01	Amphibole	Biotite	Hematite	Glass[a]
SA-123 A	1,000	72.4	14.5	2.0	0.8	0.0	10.2	0.0	0.1	0.2
SA-123 D	1,101	63.8	14.8	3.3	3.2	0.1	14.8	0.1	0.0	0.2
SA-123 E	1,022	77.3	17.3	2.9	1.5	0.5	0.5	0.0	0.0	0.2
SA-123 F	1,100	64.9	23.0	5.1	0.0	1.9	0.0	0.0	0.05	5.0
SA-123 G	1,000	76.8	15.4	0.0	0.0	4.7	0.0	0.0	0.0	3.1
SA-123 H	1,000	52.9	30.7	1.9	0.0	13.7	0.0	0.0	0.0	0.3
SA-123 I[b]	1,000	62.6	10.6	3.9	1.4	0.0	17.0	1.4	0.1	0.1
SA-123 J	1,044	55.5	33.9	6.8	3.5	0.0	0.0	0.0	0.1	0.2
SA-123 L	1,000	61.0	21.5	2.0	4.8	0.0	10.7	0.0	0.0	0.8
SA-123 M	1,000	69.4	16.5	5.1	0.0	8.6	0.0	0.0	0.1	0.4
SA-123 N	1,021	73.4	18.0	4.9	0.0	2.9	0.0	0.0	0.0	0.8

[a] Includes glass along grain boundaries and in inclusions
[b] This sample also contains 2.0% quartz

and rock types. The type 1 crystals, although not very abundant overall, are most common in the hornblende andesites. Type 2a crystals are abundant in the most vesicular samples in which they occur nearly free of the zoned outer rims particularly when directly adjacent to vesicles. They are progressively less abundant in the series andesite-basaltic andesite-basalt. Crystals of type 2b are most common in the basaltic andesites, less common in the basalts and rare in the andesites. Type 2c crystals are most abundant in the basalts, less abundant in the basaltic andesites and rare in the andesites.

Plagioclase in the gabbros is relatively homogeneous in both texture and composition. In samples lacking hydrous minerals, the plagioclase crystals are An-rich (e.g. SA-123J, SA-123H; Fig. 4), optically unzoned and show adcumulus textures. Crystals in samples containing hydrous minerals have lower An contents (e.g. SA-123L; Fig. 4) and regularly zoned rims that make up as much as 15 volume percent of the crystals.

The compositional diversity of the Sarigan plagioclase crystals is summarized in Fig. 4. Tables of plagioclase analyses are available from the authors upon request. Note that (1) type 1 crystals are the most anorthite-rich in any given sample, (2) in individual crystals inner-rims are more anorthitic than adjacent cores including those with abundant inclusions (e.g. SA-71-1), (3) inclusion-rich cores in type 2a crystals are more anorthitic than inclusion-free type 2c cores, (4) inclusion-free type 3 groundmass crystals are generally the least anorthitic crystals in a given sample and (5) the range of anorthite contents observed in individual samples increases with decreasing age of the sample.

Clinopyroxene

This is the most abundant ferromagnesian mineral in all the samples examined (Tables 1 and 2). In general, it occurs as euhedral to subhedral phenocrysts and microphenocrysts and shows no reaction relations with the groundmass (e.g. resorption, opx rims, etc.). Sparse anhedral microphenocrysts (i.e. crystal fragments) also lacking reaction rims occur in some samples. In scoriaceous samples, clinopyroxene often shows glass growth inclusions similar to those observed in plagioclase.

Although the range in composition observed within the stratigraphic sequence is rather limited, some consistent trends are evident. These are: (1) the cpx found in glomeroporphyritic clots and as anhedral microphenocrysts is generally more magnesian than that found as euhedral, isolated phenocrysts and microphenocrysts (2) clinopyroxene rims over orthopyroxene cores have compositions similar to the microphenocrysts in a given sample (Fig. 5) and (3) zoning is very limited in all analyzed samples. Pigeonite was identified as the groundmass pyroxene in only

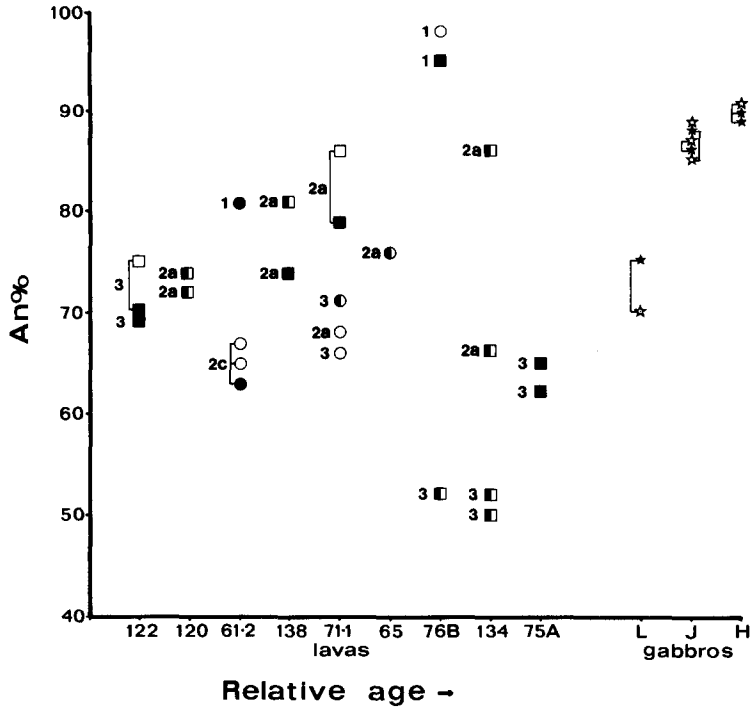

Fig. 4. Plagioclase compositions in lavas and gabbros. Lava samples are plotted against relative age of host. Symbols are keyed as follows: *square*=phenocryst; *circle*=microphenocryst; *filled symbol*=core analysis; *half-filled*=analysis between core and rim; *open*=rim analysis; *stars*=gabbro plagioclase; *numbers* refer to plagioclase crystal types discussed in text. *Line* connecting 2 analyses indicates core and rim analysis of same crystal

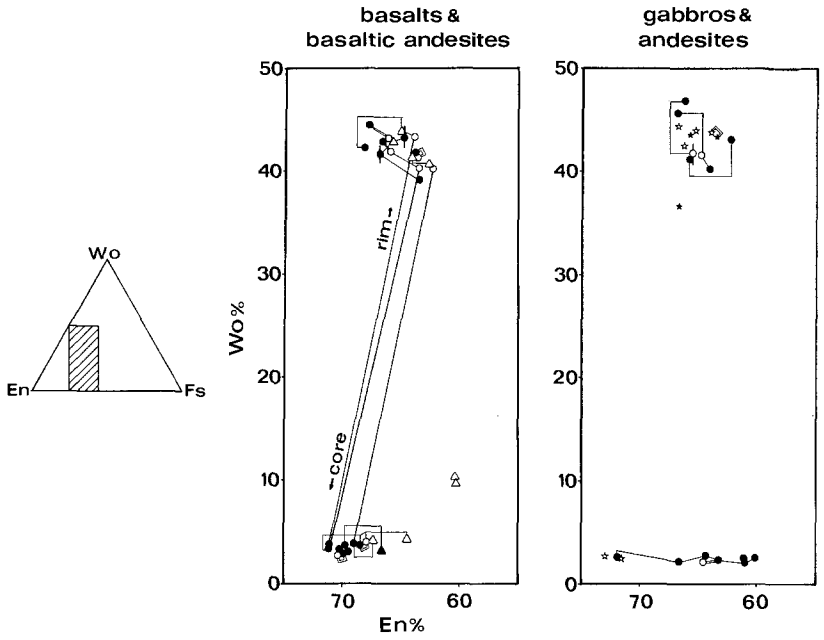

Fig. 5. Pyroxene compositions. Symbols: *circles*=phenocrysts; *triangles*=groundmass grains; *stars*=gabbro pyroxene; *filled symbol*=core analysis; *open symbol*=rim; *heavy lines* connect opx cores and cpx rims. *Light single lines* connect crystals from a single rock sample. *Double lines* connect core and rim analyses of single crystals

one sample (SA-65; Fig. 5). Tables of pyroxene analyses are available from the authors upon request.

The clinopyroxene in the gabbros is similar in composition to the phenocrysts and likewise shows very little zoning. Texturally, it shows some complex relations. In the least differentiated samples, its crystal form is similar to plagioclase suggesting these minerals crystallized at the same time. In the more differentiated samples, clinopyroxene commonly is anhedral and occurs interstitially to plagioclase, suggesting it crystallized later. Finally, in the most differentiated samples it is partially replaced by uralitic amphibole.

Orthopyroxene

This mineral displays a more complex behavior than clinopyroxene. In the basaltic andesites of the Basal Sequence (Qbs), the shoreline flows (Qsf) and the Ridge Top flows (Qrt), orthopyroxene commonly forms the cores of phenocrysts enclosed by clinopyroxene rims which form up to 50% of the volume. In the more differentiated basaltic andesites, thick rims are less abundant and thin rims ($\leq$10% by volume) are common. Finally, in the andesites, reaction rims are absent. As a groundmass phase, orthopyroxene is absent from the least differentiated basaltic

Table 3. Microprobe analyses of olivine

	Qsf SA-61-2	Qsf SA-71-1	Scoria SA-93	Qan 1 SA-76B	Qan 2 SA-134	Gabbros			
						SA-123H	SA-123H	SA-123H	SA-123D
SiO_2	37.60	36.35	38.57	40.89	39.38	37.79	37.88	37.85	38.52
TiO_2	0.03	0.00	0.04	0.17	0.02				0.03
FeO	24.74	31.01	24.96	10.88	19.38	22.66	22.75	22.46	19.63
MnO	0.45	0.45	0.36	0.30	0.34	0.50	0.44	0.46	0.81
MgO	36.25	31.63	36.49	45.98	41.01	38.45	38.39	37.71	40.73
CaO	0.17	0.25	0.25	0.22	0.15	0.16	0.16	0.15	0.05
Total	99.29	99.69	100.67	98.44	100.28	99.56	99.62	98.63	99.77
X_{Fo}	0.72	0.64	0.72	0.88	0.79	0.75	0.75	0.74	0.78
	s,m,c[a]	s,m,c	e,m,c	s,m,i	s,m,c	s,c	s,i	s,r	a,r
	0.05×0.3[b]	0.2×0.2	0.5×0.3	0.3×0.2	0.2×0.2	–	–	–	0.4×0.2

[a] First letter designates shape: a=anhedral, s=subhedral, e=euhedral. Second letter indicates whether crystal occurs in matrix (m) or in glomeroporphyritic clot (c). Third letter indicates whether analysis of core (c), intermediate between core and rim (i) or rim (r)
[b] Size in mm

andesites, equal in abundance to groundmass olivine in the more differentiated basaltic andesites, less abundant than groundmass clinopyroxene in the mafic andesites and more abundant than clinopyroxene in the siliceous andesites.

In the samples lacking hydrous minerals, orthopyroxene found in glomeroporphyritic clots, as phenocrysts and as cores mantled by clinopyroxene, show a limited compositional range (En_{66-70}; Fig. 5). The groundmass orthopyroxene in these samples ranges from En_{62} to En_{65}. Outer rims enriched in En, relative to the cores, were found in several of the more differentiated samples (Fig. 5). Such rims have been interpreted as evidence of magma mixing (e.g. Kuno 1950). The wide range of compositions shown by phenocrystic opx in the hornblende andesites also suggests a mixing process.

In the gabbros, orthopyroxene was clearly a late crystallizing phase on textural evidence. Also, since orthopyroxene and olivine are nearly mutually exclusive (Table 2), it is reasonable to assume orthopyroxene did not replace olivine until late in the crystallization sequence. The composition of orthopyroxene in the gabbros (En_{70-72}) is very similar to the mantled orthopyroxene in some of the basaltic andesites (Fig. 5).

Olivine

Although generally low in abundance (Table 2), this phase is present as euhedral to subhedral phenocrysts in most of the Sarigan lavas examined. In the basaltic andesites, the phenocrysts occasionally have a very thin rim of pyroxene granules and Fe–Ti oxide grains. In the more differentiated samples the rims are common and generally dominated by titanomagnetite. In the hornblende andesites, olivine phenocrysts are occasionally pseudomorphed entirely by titanomagnetite granules. A less common type of olivine occurrence consists of olivine grains penetrated by symplectic titanomagnetite and rimmed by orthopyroxene crystals. This type of olivine is also found in the gabbros, although rarely. Inclusions of brown spinel were not observed in any olivine crystals.

Olivine is common as a groundmass phase in the basaltic andesites but not in the andesites. As a groundmass phase, it is commonly surrounded by titanomagnetite granules in what appears to be a reaction relation. In some samples, only clots of titanomagnetite grains forming olivine outlines remain in the groundmass. These observations all sugest the Sarigan lavas were erupted under relatively high oxygen fugacities.

Analyses of olivine phenocrysts, listed in Table 3, indicate a wide range of compositions (FO_{64-88}). Olivines in the hornblende andesites have the highest forsterite contents whereas those in the basaltic andesites have the lowest. Analyses of groundmass olivines were not obtained due to the smallness of grain size.

The modal abundances of olivine in the gabbros decreases from 13.7% in the most mafic samples to 0% in more differentiated samples (Table 2). Most of the olivine grains in the gabbros are rounded and some are embayed. Analyzed crystals range in composition from FO_{74} to FO_{78}.

Amphibole

Hornblende occurs as phenocrysts in the hornblende andesites and as uralite in some of the gabbros. The phenocrysts are common hornblende in composition (Table 4) and invert to ba-

Table 4. Microprobe analyses of amphiboles

	Qan 2			Gabbros	
	SA-134a	SA-134b	SA-134c	SA-123L	SA-123L
SiO_2	47.99	47.11	44.84	50.23	49.76
TiO_2	1.23	1.50	2.88	0.99	1.13
Al_2O_3	8.10	8.10	10.50	5.92	6.10
FeO	11.92	13.23	12.58	11.48	11.59
MnO	0.42	0.47	0.44	n.d.	n.d.
MgO	14.79	14.46	13.71	17.10	16.90
CaO	10.93	10.78	10.90	11.80	11.84
Na_2O	1.63	1.81	1.67	0.93	0.95
K_2O	0.20	0.18	0.20	0.30	0.31
Total	97.21[a]	97.64	97.72	98.75	98.58
(Fe/Mg) molar	0.45	0.51	0.51	0.38	0.38
	a,m,c[b]	a,m,c	s,m,c	a,c	a,r

[a] Low totals reflect unmeasured H_2O content
[b] See Table 3

Table 5a. Microprobe analyses of titanomagnetite in lavas

	SA-122	SA-122	SA-61-2	SA-71-1	SA-93	SA-93	SA-65	SA-134	SA-134
SiO_2	0.12	0.08	0.10	0.18	0.12	0.21	0.20	0.24	0.21
TiO_2	9.67	9.93	12.71	10.75	9.48	10.31	12.86	11.50	12.21
Al_2O_3	3.71	3.71	1.79	3.11	4.42	4.48	2.64	0.91	0.85
FeO_t	78.56	77.33	75.65	79.46	74.89	76.48	75.51	77.96	76.91
MnO	0.48	0.49	–	–	0.32	0.23	–	0.64	0.83
MgO	2.72	2.68	1.59	1.32	3.24	3.17	2.20	0.70	0.77
CaO			0.05	0.02	–		–		
Cr_2O_3	0.10	0.11	0.23	0.40	0.14	0.22	0.04	0.06	0.05
Total	95.36	94.33	92.12	95.24	92.61	95.10	93.45	92.01	91.83
Fe_2O_3	47.34	45.98	–	44.53	45.01	44.86	40.59	43.33	41.89
FeO	35.87	35.95	–	39.39	34.38	36.11	38.98	38.96	39.20
Total[a]	100.10	98.92	–[c]	99.69	97.42	99.58	97.85	96.33	96.02
ulv	0.243	0.259	–	0.317	0.245	0.270	0.356	0.331	0.348
mag	0.757	0.741	–	0.683	0.755	0.730	0.644	0.669	0.652
e,m,c	s,m,c[b]	s,m,c	s,m,c	s,m,c	s,m,c	s,m,c	s,m,c	e,m,c	e,m,c
	0.05[b]	0.15	0.05	0.15	0.05	0.05	0.03	0.05	0.06

[a] Recalculated according to procedure of Anderson (1968)
[b] See Table 3 for definitions
[c] Cannot be recalculated due to alteration

Table 5b. Microprobe analyses of titanomagnetite in gabbros

	SA-123D	SA-123D	SA-123H	SA-123J
SiO_2	0.04	0.09	0.07	0.10
TiO_2	5.81	5.77	6.76	8.52
Al_2O_3	2.70	2.69	6.83	5.05
FeO_t	82.43	81.95	75.67	76.97
MnO	0.32	0.30	0.31	–
MgO	1.89	1.96	4.43	3.31
Cr_2O_3	0.05	0.06	1.18	0.09
Total	93.24	92.82	94.27	94.04
FeO	33.27	32.99	31.10	34.34
Fe_2O_3	54.62	54.39	48.42	47.36
Total	98.71[a]	98.24	99.10	98.79
ulv	0.142	0.140	0.150	0.219
mag	0.858	0.860	0.850	0.781
	a,r[b]	a,c	a,c	a,c
	0.2[b]	0.2	0.2	2.5

[a] Recalculated according to procedure of Anderson (1968)
[b] See Table 3 for definitions

saltic hornblende upon oxidation. Because they are unstable at surface conditions, nearly all have opacitic reaction rims. Some are completely recrystallized to fine grained masses of pyroxene, plagioclase and a Fe–Ti oxide phase, as noted earlier.

The amphibole in the gabbros usually replaces clinopyroxene although it is occasionally found as rims on titanomagnetite grains. Compositionally, it is in the tremolite-actinolite range. The molar Fe/Mg ratios are considerably lower (0.38–0.40) than those of the phenocrystic hornblende (0.51–0.52). Because they contain glass/vapor inclusions similar to those found in the anhydrous minerals of a given sample, it appears these amphiboles were formed, at least in part, as a result of the reaction of clinopyroxene with hydrous residual melt. If the reaction had taken place in the presence of only a vapor/fluid phase, the glassy portions of the inclusions would not have been produced. The sparse biotite in samples SA-123I and SA-123D may have a similar origin.

Titanomagnetite

This phase occurs as a microphenocryst in essentially all samples (Tables 1 and 2). It also occurs as a groundmass phase and as a breakdown product of olivine and amphibole in the lavas as discussed above. Analyses of representative crystals are listed in Table 5.

The compositions of titanomagnetite in the gabbros are somewhat different from those in the lavas presumably as a result of the higher pressures under which the gabbros crystallized (Powell 1978). The enrichment of Cr_2O_3 in sample SA-123H (Table 5) suggests this sample equilibrated with more primitive liquids (i.e. higher in Cr_2O_3) than the other samples. This is consistent with its more mafic mineralogy (Table 2) and bulk composition (Table 7). Texturally, the titanomagnetite in the gabbros occurs as (1) equant subrounded inclusions in plagioclase, clinopyroxene and orthopyroxene, (2) an anhedral late-crystallizing interstitial phase and (3) as symplectites produced by the oxidation of olivine. Because primary titanomagnetite is found in samples free of orthopyroxene and hydrous phases (e.g. SA-123H, SA-123N, SA-123F, Sa-123M; Table 2), we conclude it started to crystallize before orthopyroxene and the hydrous phases, but after clinopyroxene, plagioclase and olivine.

Alteration Minerals

Alteration is unusually limited within the sequence on Sarigan. Only 2 small altered areas, undoubtedly associated with fumerolic activity at one time, were observed on the island. Secondary minerals were observed in only 2 out of 150 thin sections; these include finely crystalline quartz in a vent sample from the surface of the lobate flows (Qlf), and clays in a breccia sample from the base of the andesite sequence on the south coast.

In summary, the petrographic and mineral chemistry data point toward a rather complex magmatic evolution for the Sarigan volcano. Similar petrographic observations have been made in other areas such as Hakone in Japan (Kuno 1950). Three lines of evidence suggest the Sarigan magmas evolved under higher f_{H_2O} than those of the other Mariana volcanoes. These are: (1) nearly all the Sarigan lavas show a high degree of crystallinity compared to lavas from other Mariana arc volcanoes (Meijer 1981a) (2) amphibole is found in the Sarigan lavas but not in lavas from the other volcanoes and (3) the Sarigan lavas contain phenocrysts of plagioclase very rich in anorthite (see Yoder 1969).

The petrographic and chemical evidence for disequilibrium detailed above including: (1) the presence of several textural types of plagioclase crystals in single samples (2) opx crystals with and without thick cpx rims, (3) reaction textures in olivine phenocrysts and (4) the coexistence in a single sample of crystals of the same mineral with distinctly different compositions, undoubtedly reflect a range of processes. The anhedral, largely unzoned, inclusion-free, anorthite-rich plagioclase crystal fragments discussed above most reasonably represent disaggregated gabbroic material since the gabbros contain crystals with the same chracteristics. This implies at least part of the cpx, olivine, opx and titanomagnetite phenocrysts and microphenocrysts in the lavas were also derived from gabbroic material. The anhedral fragments of Mg-rich cpx, opx and olivine could be explained this way. Other indications of disequilibrium conditions listed above require additional explanations.

A model involving two levels of magma storage in the crust, with repeated injection of new magma into the storage chambers, can qualitatively explain the other disequilibrium features. The model is based on the results of geophysical studies of magma chambers (e.g. Sharp et al. 1980) and recently recognized zonation effects in these chambers (e.g. Ritchey 1980). In the model, the minerals olivine, plagioclase, augite $\pm$ titanomagnetite and hypersthene crystallize from a basaltic andesite magma injected into the deeper level chamber from below. At some point in the crystallization interval, a new batch of crystal-poor basaltic magma enters the chamber from below. This magma is initially at a higher temperature than the pre-existing magma and therefore causes the phenocrysts in the latter to be partially resorbed as thermal equilibrium is attained. During equilibration, the magmas are intermixed (Anderson 1976) and cotectic crystallization is resumed at a higher temperature than before. If hypersthene had been crystallizing from the preexisting magma, it would be resorbed and would subsequently be armored by augite assuming the new equilibrium temperature exceeded the liquidus temperature of hypersthene in the magma. With further injection of new magma from below, the mixed magma in the chamber is displaced upward thru the magma conduit into shallower chambers and a cooler environment. The drop in pressure and temperature could result in rapid growth of inclusion-rich rims on preexisting plagioclase cores (type 2C) or rapid growth of inclusion-rich cores (type 2A) in those magmas poor in earlier crystallized plagioclase. The activity of water in the magma will influence the extent of rapid growth with higher water contents leading to more extensive growth. The decrease in confining pressure would cause the newly crystallized rims to be higher in anorthite than the inclusion-free cores (Yoder 1969). Continued crystallization of the magma with decreasing temperature would result in the formation of inclusion-free zoned rims over the inclusion-rich cores and rims. The ferro-magnesian minerals would also undergo additional growth during this stage.

The hornblende andesites require special consideration because, although they are relatively differentiated rocks, they lack inclusion-free plagioclase cores. Plagioclase must have been a stable phase in the andesitic magma at depth because it is a common phase in the more mafic magmas and would remain on the liquidus with differentiation. Either plagioclase crystallized in the andesitic magma at depth, became unstable for some reason, was resorbed and subsequently became stable again at shallower levels or the andesitic magma was plagioclase-poor to begin with and rapidly crystallized plagioclase after intrusion to shallow levels. The latter alternative is supported by recent studies of zonation in magma chambers. Ritchey (1980) has concluded that the magma chamber beneath Crater Lake, Oregon was zoned prior to the climactic event that formed the present caldera with a rhyolitic cap overlying a more mafic basal magma. The crystal-poor, water-rich rhyolitic cap apparently formed as a result of boundary layer flow (Turner 1980). The Sarigan andesites may have been produced by the same process. That is, as the interval of repose between eruptions increased near the end of the history of the volcano, a crystal-poor andesitic magma, relatively enriched in water, could have formed as a cap over a crystal-rich basal magma. The andesitic magma may have crystallized minor hornblende if the water content were sufficiently high, but plagioclase crystallization would be largely inhibited by high temperature and high water contents. If this magma was intruded into shallower levels, it would rapidly crystallize to produce the inclusion-rich plagioclase cores along with pyroxene $\pm$ hornblende $\pm$ olivine $\pm$ titanomagnetite. Subsequent crystallization at shallow levels would produce the zoned rims on plagioclase and other phases.

Once magmas leave the shallow chambers to erupt on the surface, decompression and cooling would result in one or more of the following: (1) at deeper levels, gabbroic wall rocks would be disaggregated and included in the magma (2) olivine would replace hypersthene as a stable groundmass mineral in the basaltic andesites and (3) at very shallow levels, olivine and amphibole (when present) would decompose to magnetite dominated assemblages.

Geochemistry

Major Elements

Selected whole-rock major and trace element analyses are presented in Table 6 in chronologic sequence (oldest on left). Sample numbers are also plotted on the Figs. 2 and 3. Whole rock analyses of gabbroic samples are listed in Table 7.

Most of the Sarigan lavas belong to the calc-alkaline series according to classification schemes currently in use (e.g. Irvine and Baragar 1971). This is well displayed in the AFM diagram shown in Fig. 6. The lack of an iron enrichment trend distinguishes these lavas from those exposed on most of the other Mariana active arc islands such as Maug (see Meijer 1981a). Several scoriaceous samples deviate from the main trends towards iron enriched compositions. These are discussed separately below.

Table 6a. Major and trace element analyses of lavas

	Qbf SA-122	Qbf SA-120	Qbf SA-123B	Qsf SA-61-2	Qsf SA-138	Qsf SA-130	Qsf SA-71-1	Scoria SA-93	Qpc SA-53	Qpc SA-52	Qrt SA-51
SiO_2	56.54	55.29	54.75	52.01	53.16	53.35	52.90	52.73	57.06	52.59	53.01
TiO_2	0.77	0.75	0.76	0.72	0.76	0.74	0.71	0.78	0.89	0.74	0.74
Al_2O_3	17.32	16.86	16.61	15.72	16.15	17.24	16.65	16.74	17.74	16.50	16.54
FeO_t	7.04	8.07	8.58	8.95	9.00	8.65	9.23	9.43	7.48	9.22	9.35
MnO	0.17	0.18	0.18	0.16	0.19	0.17	0.18	0.18	0.20	0.18	0.18
MgO	4.57	5.25	5.31	7.57	5.68	5.75	6.27	5.58	3.87	6.76	5.91
CaO	8.54	9.78	10.12	11.63	11.23	11.06	10.90	11.10	8.68	10.75	10.96
Na_2O	3.29	2.71	2.98	2.82	2.68	2.54	2.42	2.53	3.11	3.13	2.45
K_2O	1.07	0.91	0.87	0.55	0.77	0.61	0.66	0.61	0.89	0.53	0.58
P_2O_5	0.19	0.17	n.d.	n.d.	n.d.	0.11	0.14	0.12	0.15	n.d.	0.14
Total[a]	99.50	99.97	100.16	100.13	99.62	100.22	100.06	99.80	100.07	100.40	99.86
L.O.I.[b]	1.09	0.65	0.39	1.71	0.76	0.83	0.43	0.80	0.91	0.62	1.29
Molar (Mg/Fe+Mg)	0.536	0.537	0.525	0.601	0.529	0.542	0.548	0.513	0.480	0.566	0.530
Ba[c]	320	310	291	226	252	263	260	235	290	271	243
Cu	70	67	n.d.	47	102	112	77	127	101	20	105
Ni	29	15	25	33	23	32	35	26	16	33	27
Rb	22.9	20.0	17.7	9.0	11.7	10.2	11.7	11.2	14.5	9.6	10.8
Sr	410	386	385	400	384	335	392	336	345	350	340
Y	20.4	24.2	24.1	16.4	15.1	20.7	17.3	18.2	25.4	23.3	19.8
Zn	82	82	78	73	84	81	79	82	88	77	81
Zr	74.1	73.9	73.5	51.4	61.7	66.8	57.3	60.4	87.0	64.2	67.1
K/Rb	388	378	410	507	546	496	468	452	509	458	446

[a] Analyses of volatile-free aliquots. See appendix for procedures
[b] Loss on ignition in wt.%
[c] All trace element analyses by X-ray fluorescence, in ppm

Table 6b. Additional trace element analyses[a]

	SA-120	SA-130	SA-53	SA-78	SA-100	SA-54	Relative Error %
Cr	80.6	95.8	20.6	24.6	44.8	17.8	7
Sc	35.8	40.7	30.1	26.2	31.1	27.2	6
HF	n.d.	1.91	n.d.	2.40	n.d.	n.d.	10
La	9.55	6.79	7.41	7.77	7.5	7.77	4
Sm	3.13	2.18	2.94	2.94	2.94	2.94	2.5
Eu	1.02	0.95	0.96	1.02	1.00	1.02	5
Yb	2.55	2.27	2.66	3.37	3.1	3.37	4
$(La/Yb)_N$[b]	2.47	1.98	1.84	1.52	1.60	1.52	8

[a] By INAA, see appendix
[b] Chondrite normalized

Because essentially all the Sarigan lavas are porphyritic, the whole rock analyses may not represent liquid compositions. For this reason, we have analyzed the groundmass compositions in a number of samples. These are listed in Table 8.

In an attempt to identify less differentiated liquid compositions, we analyzed glass inclusions in several of the gabbro samples. The observed compositions, recalculated as volatile-free, show a clear trend from andesite to rhyolite in progressively more differentiated gabbros (see Table 9). Compositions of liquids that were less differentiated than any of the lavas were not found.

Isotopic Compositions

The distinctive Fe trend of the Sarigan lavas compared to lavas from the other islands is not reflected in the isotopic compositions of the elements Nd, Pb and Sr. As noted by DePaulo and Wasserburg (1977), the $^{143}Nd/^{144}Nd$ and $^{87}Sr/^{86}Sr$ ratios of Sarigan lavas (Table 10) are similar to those observed in lavas from Agrigan (Fig. 1) and as a group these fall in the range of oceanic island (e.g. Hawaii) lavas. Two new Sr isotopic analyses are listed in Table 10; one for a basaltic andesite (SA-61-1) the other for a hornblende andesite (SA-78). These analyses are identical within experimental error and similar to earlier analyses (Table 10). They provide no evidence for a high $^{87}Sr/^{86}Sr$ component (e.g. seawater or oceanic sediment) in the Sarigan magmas. A new Pb isotopic analysis is also listed in Table 10. Although it is the most radiogenic active arc sample analyzed to date (Meijer 1976), it is within experimental error of the ocean basin field and plots directly on a regression line with other lavas from the Mariana arc systems (Fig. 7). The isotopic data thus point to a mantle source for the Mariana arc lavas either through a single stage or multi-stage process (Ringwood 1974).

Table 6a (continued)

Qrt SA-96	Qrt SA-98	Qrt SA-65	Qan-1 SA-78	Qan-1 SA-76B	Qan-2 SA-134	Qan-2 SA-75A	Qan-3 SA-58	Qnf SA-100	Qsd SA-142	Qd SA-124	Qlf SA-54	
52.76	52.84	55.09	59.09	59.92	61.05	61.02	59.27	55.94	58.25	60.10	58.75	±0.15
0.76	0.78	0.84	0.78	0.71	0.70	0.70	0.69	0.69	0.73	0.77	0.83	±0.03
16.27	16.98	17.48	16.68	16.65	16.36	16.52	16.11	17.39	16.39	16.32	16.77	±0.15
8.94	9.17	9.04	7.31	6.55	6.40	6.30	6.57	8.00	7.05	6.63	7.60	±0.10
0.17	0.17	0.18	0.19	0.15	0.15	0.14	0.15	0.17	0.16	0.15	0.19	±0.01
6.62	5.95	4.32	3.31	3.20	2.76	2.66	4.45	4.17	3.89	3.31	3.92	±0.10
10.65	10.81	8.89	7.40	7.33	6.99	7.00	8.55	8.73	8.30	8.15	8.11	±0.10
2.81	2.97	2.77	3.44	4.16	3.99	3.90	3.04	3.05	3.90	3.50	3.08	±0.10
0.70	0.70	0.90	0.89	1.05	0.93	1.06	0.92	0.83	0.80	0.90	0.81	±0.02
n.d.	0.13	0.18	0.14	n.d.	n.d.	n.d.	n.d.	0.18	n.d.	n.d.	n.d.	±0.02
99.68	100.50	99.69	99.23	99.72	99.33	99.30	99.75	99.15	99.47	99.83	100.06	
0.67	0.91	1.10	1.43	1.54	0.71	0.64	0.95	1.22	0.59	1.39	1.06	
0.569	0.536	0.460	0.447	0.465	0.435	0.429	0.547	0.482	0.496	0.471	0.479	
244	262	282	330	294	345	352	288	292	298	290	321	±7
98	100	63	57	58	45	55	75	99	74	57	76	±4
25	32	21	14	4	5	5	22	11	15	21	16	±3
9.8	11.0	10.0	15.5	16.2	16.7	16.1	13.9	15.0	14.3	16.0	15.4	±1.0
351	342	369	336	371	360	354	353	336	380	373	373	±6
16.4	19.6	25.7	28.6	25.2	22.8	22.8	23.1	23.9	21.4	25.4	21.8	±1.0
75	80	89	69	73	65	67	72	87	68	65	59	±3
56.5	71.9	80.0	91.6	82.2	86.2	88.2	76.8	80.3	83.2	81.8	85.6	±2
593	528	747	477	538	462	546	549	459	464	467	437	

Table 7. Major element analyses of gabbros

	SA-123A	SA-123D	SA-123E	SA-123F	SA-123G	SA-123H	SA-123I	SA-123J	SA-123L	SA-123M	SA-123N
SiO_2	47.06	46.67	44.94	41.97	45.22	45.08	53.26	41.03	50.48	42.01	40.66
TiO_2	0.62	0.88	0.33	0.80	0.43	0.41	0.79	1.55	0.71	0.69	0.55
Al_2O_3	20.51	18.65	23.62	21.08	22.23	15.90	16.15	17.39	16.12	19.65	22.22
FeO_t	8.84	11.78	6.36	11.05	8.30	10.32	10.37	17.51	9.98	12.91	12.33
MnO	0.14	0.20	0.10	0.14	0.13	0.19	0.18	0.23	0.24	0.12	0.12
MgO	5.73	7.73	6.28	7.44	7.35	12.09	6.26	6.96	7.17	7.45	7.69
CaO	14.82	12.94	16.69	15.83	16.39	14.50	11.02	14.23	12.55	15.95	15.48
Na_2O	1.29	1.50	1.33	1.26	0.76	0.58	2.02	0.76	1.95	0.65	0.57
K_2O[b]	0.13	0.10	0.038	0.057	0.040	0.041	0.445	0.016	0.226	0.028	0.020
P_2O_5	0.07	0.06	n.d.	n.d.	n.d.	n.d.	n.d.	n.d.	n.d.	n.d.	0.05
Total[a]	99.21	100.51	99.69	99.63	100.85	99.11	100.50	99.68	99.43	99.46	99.69
L.O.I.[a]	0.69	1.08	0.67	0.34	0.64	0.90	1.08	0.74	0.86	1.18	0.38
Molar (Mg/Fe+Mg)	0.536	0.539	0.638	0.545	0.612	0.676	0.518	0.415	0.562	0.507	0.526
Ba	99	101	84	54	39	35	163	27	123	47	20
Cu	25	36	8	93	26	30	220	85	29	n.d.	26
Ni	10	29	21	15	42	144	17	7	16	39	6
Rb	2.8	1.6	0.5	1.2	1.0	0.9	13.4	0.2	4.2	0.8	0.6
Sr	366	333	412	375	387	310	287	332	390	329	364
Y	3.0	8.0	3.0	4.0	6.0	7.0	17	4	11	3	4
Zn	61	81	31	50	40	50	62	89	65	52	69
Zr	11	15	4.0	5.8	2.5	6	56	1	19.4	4.9	0
K/Rb	385	512	631	394	331	378	276	664	447	291	277

[a] See Table 6

[b] K_2O by high precision atomic spectrophotometry

Low $\bar{D}^{s/l}$ Elements

Because low $\bar{D}^{s/l}$ elements are essentially excluded from the crystalline portion of a magma, their concentration will gradually increase in the liquid during crystallization. Figure 8 shows that the concentrations of low $\bar{D}^{s/l}$ elements such as K, Rb, Zr and Ba do not increase systematically in progressively younger Sarigan lavas. This is true even if the whole-rock concentrations are "corrected" for their phenocryst contents (Fig. 8). Several reversals are evident in the figure and others may have occured

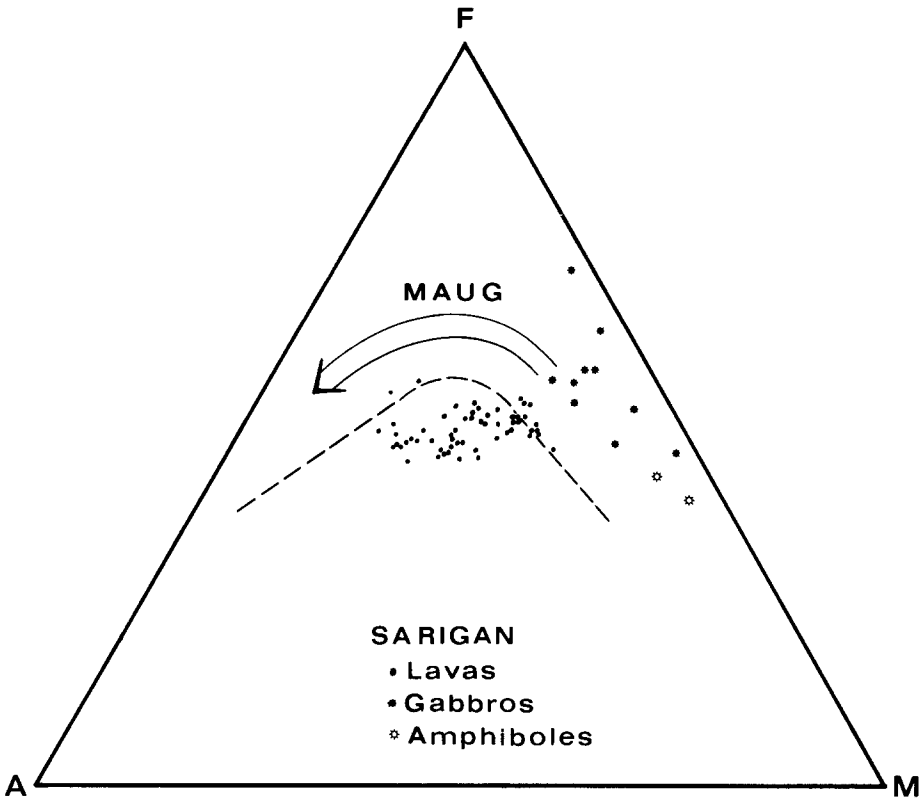

Fig. 6. AFM diagram showing whole rock composition in terms of $Na_2O+K_2O=A$, total iron as FeO=F and MgO=M. *Dashed line* represents boundary between calc-alkaline and tholeiitic series derived by Irvine and Baragar (1973). Trend of analyses of samples from Maug Island (Fig. 1) representative of tholeiitic arc series in Mariana arc, Meijer (1981). Note amphiboles in hornblende andesites cannot produce Sarigan calc-alkaline trend

Table 8. Average microprobe analyses of groundmass compositions

	Qrt SA-65	Qan 1 SA-76B	Qbs SA-86	Scoria SA-93	Qbs SA-120	Qbs SA-122	Qan 2 SA-134
SiO_2	68.34	63.02	65.80	56.49	60.39	63.26	72.52
TiO_2	1.20	0.75	0.67	1.25	0.45	0.65	0.54
Al_2O_3	13.22	18.57	17.94	15.63	19.84	17.32	12.56
FeO_t	6.80	4.41	3.81	11.26	4.04	4.66	2.95
MnO	0.13	0.10	0.02	0.23	0.06	0.10	0.16
MgO	0.98	0.74	1.17	3.44	1.99	1.24	1.94
CaO	3.56	4.88	4.35	7.79	5.64	5.10	2.57
Na_2O	4.03	3.81	3.54	3.06	3.74	4.37	3.18
K_2O	2.05	1.77	2.44	1.13	1.46	1.63	1.43
P_2O_5	n.d.	0.13	0.05	n.d.	0.21	n.d.	0.13
Total[a]	100.31	98.18	99.79	100.28	97.82	98.33	97.98

[a] Low totals due primarily to unmeasured volatile contents

Table 9. Average microprobe analyses of glass inclusions in gabbros

	SA-123G	SA-123H	SA-123J	SA-123L
SiO_2	63.09	60.02	63.71	78.61
TiO_2	1.02	0.79	0.81	0.32
Al_2O_3	17.77	20.00	17.78	14.89
FeO_t	6.34	6.54	6.81	1.82
MnO	0.15	0.11	0.20	0.08
MgO	1.00	2.24	2.17	0.39
CaO	6.50	5.75	5.53	1.95
Na_2O	3.47	3.60	2.53	0.90
K_2O	0.66	0.95	0.44	1.04
Total[a]	100.00	100.00	99.98	100.00
Host crystal:	cpx	cpx	cpx	plag

[a] Recalculated volatile-free

that are not represented in our sample population. These observations indicate the lavas exposed on Sarigan cannot all have been derived from a single magma batch. A minimum of 5 magma "batches" are required to explain the observed variations. Similar observations have been made in recent studies of other arc volcanoes (e.g. Katsui et al. 1975; Ando 1975; Condie and Swenson 1973; Rose et al. 1977; Nelson 1980; Woodruff et al. 1979; Luhr and Carmichael 1980).

The existence of 5 or more magma "batches" does not necessarily mean the crystallization history of the Sarigan lavas cannot be defined. As long as each new batch was of the same chemical type and crystallized under the same conditions, mass balance calculations such as those of Wright and Doherty (1970) will provide satisfactory estimates of the crystalline phases separated from the magma to produce the observed chemical variations in the lavas.

Ratios of very low $\bar{D}^{s/l}$ elements are useful in testing whether lavas in a given sequence could be of the same chemical type because these ratios will be essentially invariant during crystal fractionation. Several low to very low $\bar{D}^{s/l}$ elements are plotted relative to Zr ($\bar{D}^{s/l} \cong 0.05$; Pearce Norry 1979) in Fig. 9. With the exception of the Qbs samples, most samples are within analytical error of the regression lines drawn on the diagrams. This suggests the post-Qbs lavas could be cogenetic in the sense of having been derived from the same magma type while the Qbs lavas were derived from a somewhat different magma type.

Plots for Ba – Zr and Y – Zr indicate Ba and Y do not behave as true incompatible elements since regression lines through the data points do not intersect the origin. This is consistent with the fact that plagioclase and clinopyroxene, major phases fractionated from the Sarigan magmas, have significant although low distribution coefficients for Ba (0.02–0.4) and Y(0.02–0.4)

Table 10. Compilation of isotopic data for Sarigan Island

	$(^{87}Sr/^{86}Sr)i$		$(^{143}Nd/^{144}Nd)i$
S-3[a]	0.70336		–
MAR-2[b]	0.70339		0.52249
SA-61-1[c]	0.70344 ± 0.0001		–
SA-78[c]	0.70332 ± 0.0001		–
	$^{206}Pb/^{204}Pb$	$^{207}Pb/^{204}Pb$	$^{208}Pb/^{204}Pb$
SA-78[d]	18.932	15.564	38.405

[a] Data from Dixon and Batiza (1979). Not known whether value listed has been corrected for analytical bias thru either Eimer and Amend $SrCO_3$ or NBS-987

[b] Data from DePaulo and Wasserburg (1977). Normalized to Eimer and Amend $^{87}Sr/^{86}Sr = 0.70800$ using normalization procedure given in DePaulo and Johnson (1979)

[c] Normalized to $^{86}Sr/^{88}Sr = 0.1194$ and E and A = 0.70800

[d] See Meijer (1976) for analytical and normalization procedures

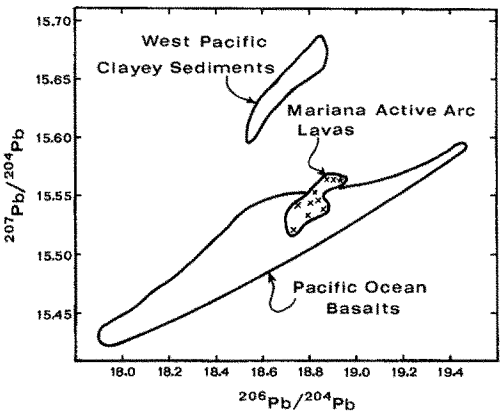

Fig. 7. Pb isotope diagram. Sarigan analysis shown as *star*. Analyses of other Mariana active arc samples represented by *X symbols*. *Boundary lines* for western Pacific sediments and Pacific Ocean basalts from Meijer (1976)

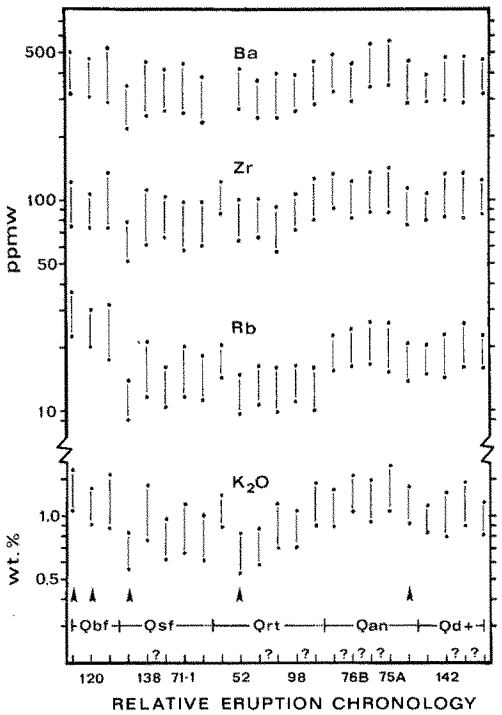

Fig. 8. Incompatible element concentrations vs. relative age of eruption. No attempt made to represent volume of material represented by single sample or volume of material not represented. *Lower point* for each element in each sample represents whole rock analysis. *Upper point* represents whole rock analysis corrected for phenocryst content to obtain closer approximation to liquid compositions. *Question marks* between samples indicate relative age designations of immediately adjacent samples are uncertain. *Arrows* represent minimum number of magma batches required to explain incompatible element variations acknowledging the uncertainties in relative age designations and possible magma chamber zoning. Not all samples plotted are numbered on abscissa

(Arth 1976). The fact that the gabbroic cumulates plot along the trends defined by the lavas is also consistent with these observations.

An important observation with regard to the origin of the hornblende andesites is that these lavas have higher K/Rb ratios than most of the other samples (Table 6). This discounts models in which the andesites are derived from the more primitive lavas by crystal fractionation of amphibole as discussed below.

Analyses of REE listed in Table 6b indicate the Sarigan magmas have $(La/Yb)_N$ ratios that range from 2.5 to 1.5 times the chondritic value. Even with the experimental error taken into account, a clear correlation exists between age of eruption and the value of the ratio as shown in Table 6b. The data imply that the younger lavas (i.e. magma batches) were derived from slightly more depleted source materials than the older lavas or by somewhat larger degrees of partial melting of the same source material.

High $\bar{D}^{s/l}$ Elements

Variations in the concentration of "high" $\bar{D}^{s/l}$ elements (i.e. $\bar{D}^{s/l} \geqq 0.5$) in cogenetic magmas reflect the mineralogic compositions of the crystalline residues from which the magmas were separated. Sato (1977) and others have pointed out that magmas in equilibrium with ultramafic mineral assemblages in the mantle have Ni/Mg ratios in the range of 0.004–0.006. Because all of the analyzed Sarigan lavas have Ni/Mg ratios less than 0.0015, they must have experienced substantial crystal fractionation prior to eruption if they were derived from the mantle.

The high $\bar{D}^{s/l}$ elements also provide a means of testing whether or not the gabbros could be related to the lavas. From data on the mineralogic composition (Table 2) and concentrations of high $\bar{D}^{s/l}$ elements in the gabbros and estimates of the appropriate mineral/liquid distribution coefficients derived from the literature (Gill 1978), the concentrations of high $\bar{D}^{s/l}$ elements in liquids with which the gabbros last equilibrated, can be approximated using the following equation:

$$C_i^l = C_i^s/(X^{cpx}D_i^{cpx/l} + X^{ol}D_i^{ol/l} + X^{plag}D_i^{plag/l} + X^{opx}D_i^{opx/l} + X^{Fe-Ti}D_i^{Fe-Ti/l} + X^{hbd}D_i^{hbd/l})$$

where C_i^s is the concentration of the element in the gabbro, X's are weight fractions of mineral phases in the gabbros and $\bar{D}_i^{s/l}$ are mineral/liquid distribution coefficients. Implicit in this equation is the assumption that liquid and crystals were in total equilibrium during crystallization. Because optical zoning is very limited in the gabbros, this would appear to be a reasonable approximation. If surface equilibrium crystallization was assumed, the calculated liquid concentrations would be somewhat lower. In the calculations, an adjustment was made for crystallization of trapped liquid by normalizing the K_2O abun-

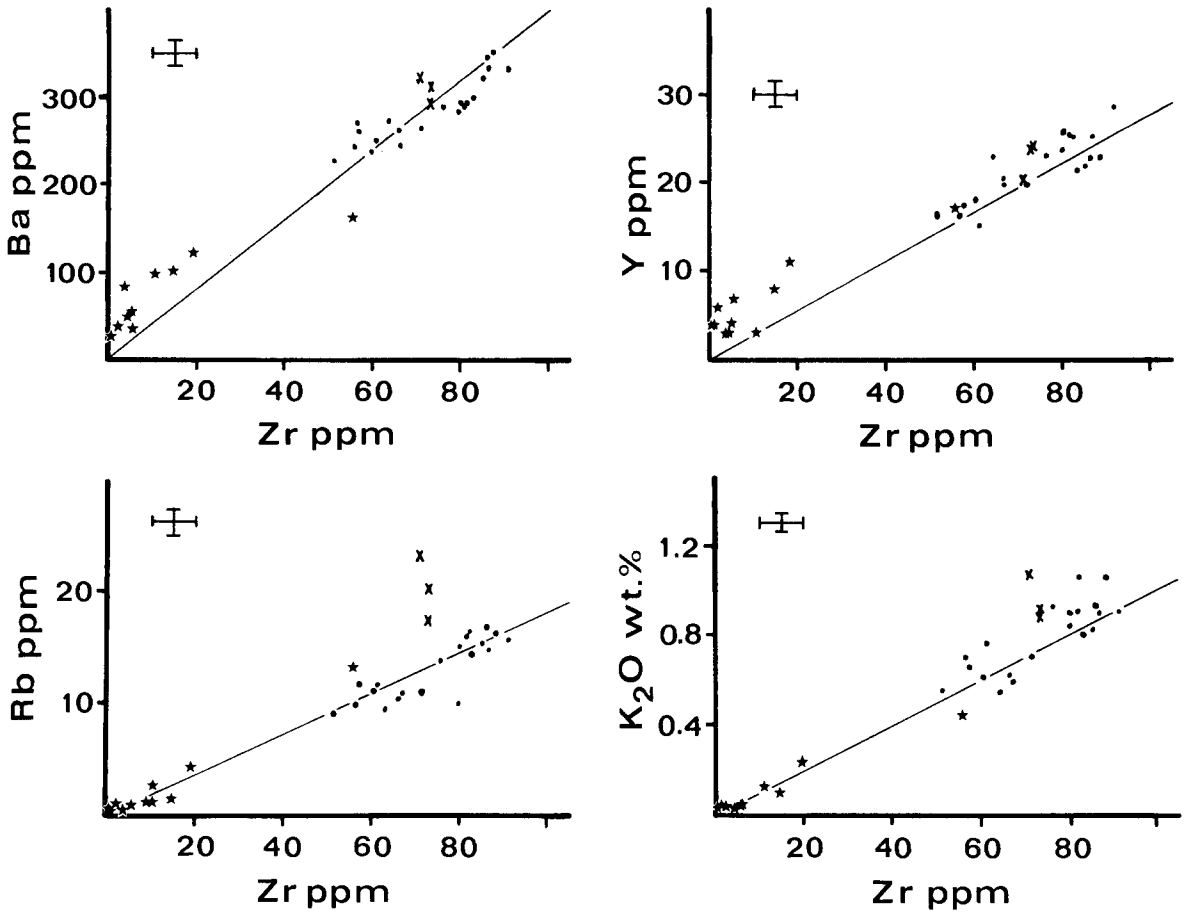

Fig. 9. Low $\bar{D}^{s/l}$ element plots. *Trend lines* represent ratios of 4.0 for Ba/Zr, 0.18 for Rb/Zr, 0.28 for Y/Zr and 83 for K/Zr. Qbs samples denoted by *X symbol*, younger lavas by *dots* and gabbros by *stars*. Error bars represent estimated total errors in analyses

dances of each gabbro to 0.02 weight percent (lowest value obtained) and assuming the residual liquids had a K_2O abundance of 1.50 wt.% (average high value in inclusions and groundmass, Tables 8 and 9). The calculated amounts of trapped liquid are small and proportional to the abundance of hydrous phases present in the samples.

The calculated liquid concentrations for Ni and Sr are plotted in Fig. 10 along with measured whole-rock concentrations in the gabbros and lavas. When compared with the lavas, most of the calculated Ni and Sr concentrations are seen to be similar to concentrations in the andesites with Zr > 80 ppm. This is consistent with the conclusion reached on the basis of glassy inclusion data as discussed above. Gabbro sample SA-123H probably equilibrated with more mafic melts than the others as shown in the Ni vs Zr, and MgO vs Zr plots.

The economically important elements Cu and Zn show very different behavior patterns. Zinc shows a slight initial enrichment followed by an almost monotonic depletion (Fig. 10). Its behavior is similar to that of TiO_2 and both can adequately be explained by fractional crystallization of the gabbroic compositions as shown in Fig. 10. This is clearly not true for Cu which shows a very erratic distribution pattern among the lavas and gabbros. There is some suggestion of depletion of Cu in the more differentiated lavas but the trend is not well defined. In general, the gabbros do not appear to be a major sink for Cu except perhaps for sample SA-123I. This sample has the highest Cu content measured but also contains the most obvious evidence of interaction with water-rich fluids as shown by the presence of fine-grained secondary tremolite, biotite and minor accessory phases (Table 2). It is possible, therefore, that the high Cu content of this sample was the result of a later hydrothermal event. The erratic distribution of Cu in the lavas cannot be adequately explained with the data available to us at the present time.

Discussion

Origin of Calc-Alkaline Fractionation Trends

The identity of the processes that produce calc-alkaline chemical trends in arc lavas has been a controversial issue since the trends were first recognized. Two related trends are generally associated with the differentiation of calc-alkaline magmas: (1) a lack of Fe enrichment (i.e. nearly constant Fe/(Fe+Mg) and (2) enrichment in SiO_2. Of the processes that have been postulated to control the calc-alkaline trends, fractional crystallization of magnetite or amphibole appear to be the most significant.

Amphibole fractionation has been proposed mainly on the basis of experimental studies. Eggler and Burnham (1973), Holloway and Burnham (1972), Helz (1976), Allen and Boettcher (1978), Cawthorn and O'Hara (1976) and others have shown that amphibole is a stable phase in basaltic to andesitic magmas under certain physical conditions. However, several lines of evidence suggest amphibole is not the phase responsible for the calc-alkaline trends observed in arc lavas. First of all, the Fe/Mg ratios of amphiboles produced in experimental studies on arc

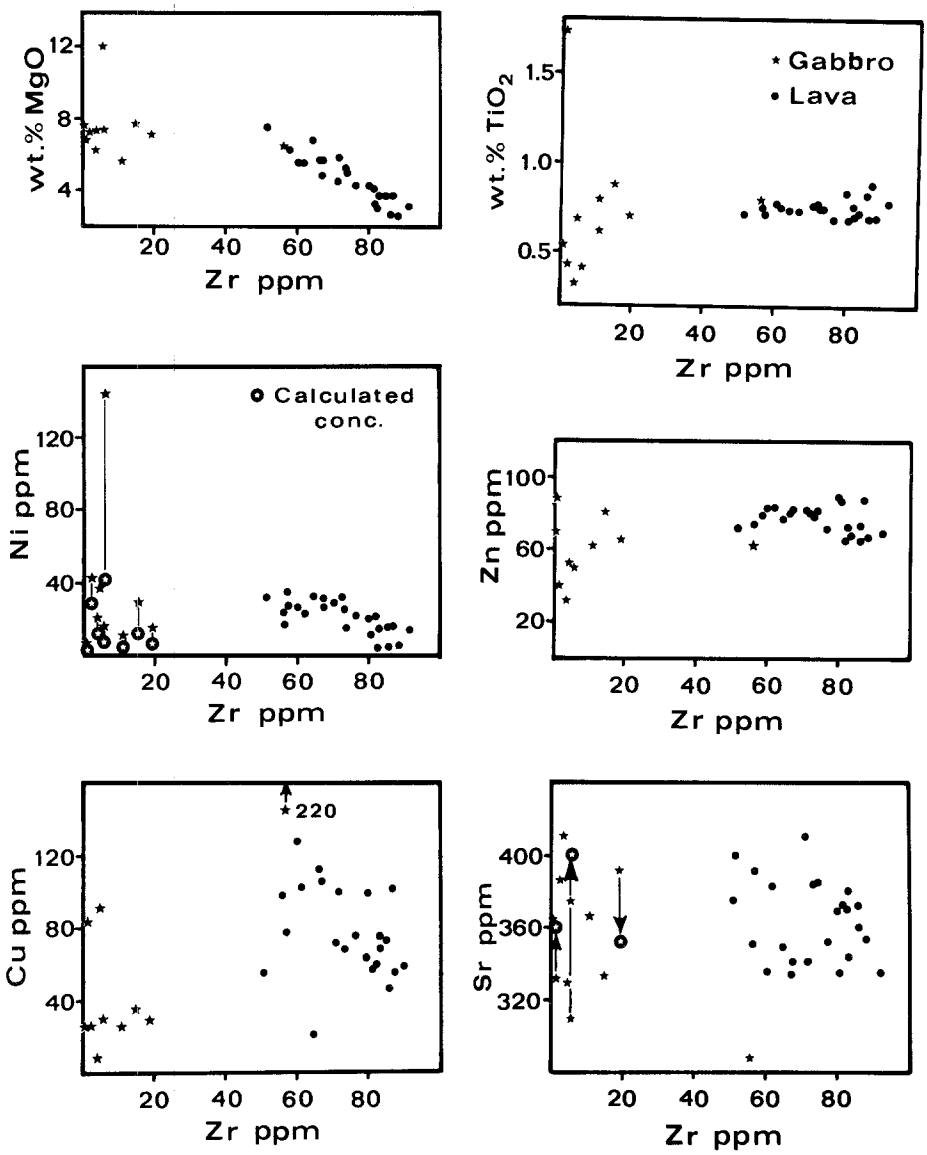

Fig. 10. High $\bar{D}^{s/l}$ element versus differentiation index as represented by Zr concentration

lavas are too low, in general, to control the calc-alkaline iron trend. In fact, Allen and Boettcher (1978; p. 1084) state "fractionation of these amphiboles over a range of f_{O_2} and f_{H_2O} could very well contribute the tholeiitic trend of early iron enrichment." Secondly, amphibole is not an abundant phase in calc-alkaline volcanic rocks (not any more abundant than magnetite; Ewart 1976). Although Stewart (1975) concluded the general lack of amphibole may be explained if the glomeroporphyritic clots of pyroxene, plagioclase, and titanomagnetite commonly observed in arc lavas are the result of low pressure decomposition of amphibole, textural relationships do not support this conclusion (Garcia and Jacobson 1979; this work). Thirdly, the measured and calculated pre-eruption temperatures of calc-alkaline andesites are generally higher than the maximum temperature stability of amphiboles in the appropriate liquid compositions (e.g. compare Fudali 1965; Eggler 1972; Eggler and Burnham 1973; Allen and Boettcher 1978; Luhr and Carmichael 1979).

Pre-eruption temperatures for a number of Sarigan lavas, calculated on the basis of the 2-pyroxene geothermometer of Wood and Banno (1973) as modified by Wells (1977), are listed in Table 11. Lavas lacking hydrous phases all yield temperatures close to 1,000° C. This temperature exceeds the maximum temperature at which amphibole is stable (at crustal pressures) in the andesitic to dacitic groundmass compositions in these samples (Table 10) by 40° to 50° C (Eggler 1972; Holloway and Burnham 1972; Eggler and Burnham 1973; Allen and Boettcher 1978). In contrast, the hornblende andesites yield temperatures around 970±20° C, consistent with the experimental results.

Table 11. Calculated pre-eruption crystallization temperatures[a]

Basaltic Andesites –		
SA-138	(Qsf)	1,001° C
SA-61-2	(Qsf)	1,013° C
SA-93	(Scoria)	1,040° C
Pyroxene Andesites –		
SA-120	(Qbs)	1,037° C
SA-122	(Qbs)	1,000° C
Hornblende Andesites –		
SA-134	(Qan 2)	984° C
SA-76B	(Qan 1)	949° C
SA-75B	(Qan 2)	979° C
Gabbro (hornblende-free) –		
SA-123J		991° C

[a] Using Wood and Banno (1973) geothermometer as modified by Wells (1977)
Estimated error ±25° C

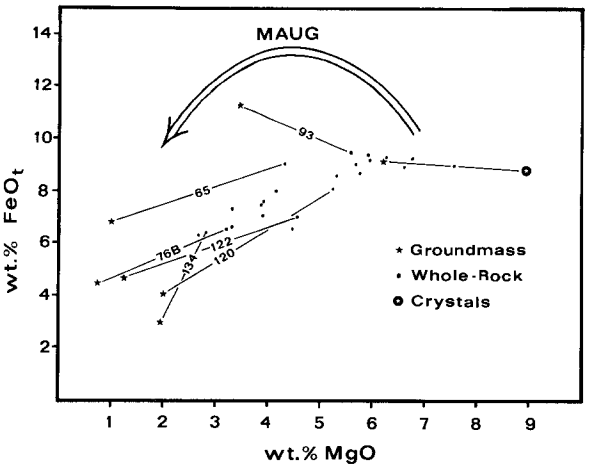

Fig. 11. FeO_{total} versus MgO diagram. Maug data from Meijer (1981)

In the case of the Sarigan lavas, K/Rb ratios also argue against amphibole fractionation as noted above. Because amphibole preferentially includes K over Rb ($D_K^{s/l}/D_{Rb}^{s/l}=2.5$; Philpotts and Schnetzler 1970) fractionation of amphibole should result in lower K/Rb ratios in residual magmas. The data listed in Table 6 indicate that the K/Rb ratios of the andesites (Qan) are equal to or greater than those of the less differentiated lavas.

Control of the calc-alkaline trends by magnetite fractionation has been advocated by Osborn (1959, 1962, 1976) mainly on the basis of phase relations in the system $MgO-FeO-Fe_2O_3-SiO_2$ under various partial pressures of oxygen. According to Osborn (1959), residual liquids formed by the fractional crystallization of basaltic magmas will become either depleted or enriched in iron depending on whether crystallization takes place with the system open or closed to oxygen. If f_{O_2} remains at a constant value during crystallization (i.e. O_2 is added to system), the residual liquid compositions will follow the calc-alkaline trends of Fe depletion and SiO_2 enrichment. The addition of anorthite to the $MgO-FeO-Fe_2O_3-SiO_2$ system does not alter the phase relations significantly (Roeder and Osborn 1966).

Objections to Osborn's model have come from several areas. Field studies (e.g. Carmichael and Nicholls 1967) note the absence or low abundance of a Fe–Ti oxide phase in samples representing the early stages of the fractionation sequence where Osborn's model would predict the highest abundance of this phase. Laboratory studies have found that under oxygen fugacities near the QFM buffer magnetite is not a near liquidus phase in lavas of intermediate composition (i.e. andesite) and could not therefore control the iron trend (Eggler 1972; Eggler and Burnham 1973). Finally, theoretical calculations indicate it is highly unlikely that calc-alkaline magmas crystallize under constant f_{O_2}. Instead, the calculations point to a regular decrease in f_{O_2} with decreasing temperature as a result of buffer reactions (Presnall 1966; Eggler and Burnham 1973; Mueller and Saxena 1977).

In spite of these objections, a rather good case can be made for titanomagnetite control of the calc-alkaline trends in the Sarigan lavas. In thin section, titanomagnetite is a ubiquitous microphenocrystic phase in all the Sarigan samples studied. The microphenocrysts are generally euhedral to subhedral and comprise 0.5–2.5 volume percent of the samples (Table 1). Titanomagnetite is also a common phase in the gabbros (Table 2) which argues for its stability during crystallization of the magmas at depth. Although amphibole is also found in some of the gabbros (Table 2) it is uralitic and has FeO/MgO ratios (Table 6) that are too low to produce the calc-alkaline iron trend as noted above (Fig. 6; Allen and Boettcher 1978).

The presence of titanomagnetite as a microphenocryst phase overcomes the objections of Carmichael and Nicholls (1967) but does not in itself prove this phase produced the calc-alkaline trend. A critical step in this direction would be to document that the groundmass composition of each of the progressively more differentiated lavas also followed the calc-alkaline trend, that is, to rule out the possibility that the calc-alkaline trend of the (porphyritic) whole rock analyses was simply a fortuitous result of dilution of iron-enriched liquids by iron-poor phenocrysts (e.g. plagioclase and Mg-rich orthopyroxene). This is shown in Fig. 11. The most important result on the diagram is that the lines connecting whole rock, groundmass and bulk phenocryst analyses, defining the liquid line of descent, generally follow the calc-alkaline trend. This implies that the observed phenocryst assemblages (including titanomagnetite) did indeed separate as a group (as opposed to differential separation) from the more mafic magmas to produce the less mafic magmas.

The groundmass compositions for the scoriaceous samples (e.g. SA-93) deviate from the main trend toward more iron-rich compositions although the whole rock analyses for these samples are the on main trend. We suggest this deviation may be due to reduction of these samples by H_2 diffused from the main magma body just prior to eruption. The change in f_{O_2} stimulated by this mechanism could displace titanomagnetite from the crystallization sequence resulting in Fe enriched residual liquids. The loss of oxidized sulfur from the magma as SO_2 (Anderson and Wright 1972) could also produce the observed trend.

In evaluating the experimental results of Eggler (1972) and Eggler and Burnham (1973) in light of the conclusions reached in this study, two factors should be considered. One concerns the starting material used in the experimental work. Eggler and Burnham (1973) state the andesite they used contained phenocrysts of plagioclase and orthopyroxene. Because phenocrysts are difficult to distinguish from xenocrysts, it is possible their starting composition was not a true liquid composition and should therefore not be used to model phase stabilities.

The second and probably more important factor concerns the f_{O_2} in calc-alkaline magmas during fractional crystallization. As noted above, Eggler and Burnham (1973) found magnetite was not a liquidus phase in their andesitic starting composition at f_{O_2} of the QFM buffer and could therefore not control the iron-enrichment trend. However, Holloway and Burnham (1972; Fig. 3) found, in their study of the hydrous melting behavior of a tholeiitic basalt, that magnetite was a stable phase in andesitic melts at f_{O_2} of the Ni–NiO buffer. This and similar data from other studies (e.g. Ritchey and Eggler 1978) indicate that magnetite stability in mafic magmas is very sensitive to $(f_{O_2})_{magma}$ in the range of the Ni–NiO buffer.

We have calculated values for (f_{O_2}) in a number of Sarigan samples over a range of total pressures using the following equilibrium relation:

$$\underset{\text{olivine}}{6Mg_2SiO_4}+\underset{\text{opx}}{6FeSiO_3}+\underset{\text{gas}}{O_2}=\underset{\text{titan-mt}}{+2Fe_2O_3}+\underset{\text{opx}}{12MgSiO_3}$$

and the coefficients derived by Luhr and Carmichael (1980). The calculated values are generally 2–3 log units higher than the QFM buffer. They are in the high end of the range reported by Fudali (1965) and similar to values reported by Luhr and Carmichael (1980) for andesites from Volcan Colima in Mexico. Our conclusion is that the "elevated" f_{O_2} in the Sarigan magmas

caused titanomagnetite to be a stable phase early in their crystallization history thereby controlling the Fe-enrichment trend.

Experimental Procedures

Phenocryst, microphenocryst, and matrix compositions were determined using a ARL-SEMQ electron microprobe. Whole rock major element analyses were also analyzed on the microprobe following a Mo strip-furnace fusion. The microprobe procedures are described in detail in Meijer et al. (1981). Neutron activation analysis closely followed the procedures published by Jacobs et al. (1977). The Pb and Sr isotope procedures are detailed in Meijer (1976).

Procedures for the X-ray fluorescence analysis of trace elements require further explanation. All analyses were performed on whole-rock sample powders (6–7 grams) pressed into 2.5 × 0.7 cm round pellets containing 10–15 drops of a saturated polyvinyl alcohol binder solution. All X-ray data were corrected for secondary absorption by measurement of the compton scattered MoK$_\alpha$ line. The Zr and Y line intensities were corrected for interference by Rb and Sr K$_\beta$ lines. Instrumental drift was monitored by repeated analysis of a reference sample. Errors listed in Table 6a represent estimates of the total analytical error (2σ).

Conclusions

Lavas erupted on Sarigan Island have chemical, mineralogic and textural characteristics common to lavas erupted in many continental volcanic arcs; they follow calc-alkaline fractionation trends and contain hydrous phases. Combined with the lack of evidence in the Pb, Sr and Nd isotope ratios for continentally derived components, these observations indicate that calc-alkaline magmas can be generated directly from mantle sources.

Trace element and minor element data indicate the Sarigan lavas were derived from five or more magma batches. All except those represented by the earliest flow sequence (Qbs) could have been derived from similar source materials based on incompatible element and isotope ratios. Major and trace element data also indicate that gabbros included in the pyroclastic breccias crystallized from magmas very similar in compositions to those comprising the post-Qbs flow units.

Petrographic and chemical data combined suggest the following crystallization sequence: olivine – plagioclase – clinopyroxene – titanomagnetite – orthopyroxene – hornblende ± accessory phases. Although the early crystallization of olivine, plagioclase and clinopyroxene produced an initial iron-enrichment in the magmas this was reversed once titanomagnetite began to crystallize. As the activity of silica in the liquid increased with the crystallization of titanomagnetite, orthopyroxene became a stable phase replacing olivine. Decreasing temperatures (< 950° C) and increasing P_{H_2O} eventually led to the crystallization of hornblende, and in the gabbros, biotite with hornblende (uralite).

The fractional crystallization of titanomagnetite appears to have been the crucial factor in development of calc-alkaline trends in the Sarigan lavas. Titanomagnetite stability was enhanced by relatively high f_{O_2}, high f_{H_2O} and low crystallization temperatures (1,020 ± 30° C).

Acknowledgements. We would like to express our gratitude to all the individuals who made this study possible. J. Villagomez and his associates in the Government of the Northern Marianas were very helpful in arranging the logistics for our field work. Elizabeth Anthony and Steven Rooke assisted in the field work and the subsequent laboratory analyses along with J.M. Haney, J. Bloom, D. Currier and other students at the University of Arizona. Tom Teska and Dr. M. Drake provided and maintained the microprobe facilities. Leslie Stanley, Jo Ann Overs, and Doris Edwards typed and edited the manuscript. Reviews of the manuscript by A.T. Anderson, M.O. Garcia, C.A. Hopson, and J. Luhr are gratefully acknowledged. This work was supported by the National Science Foundation under grant no. OCE-78-6760.

References

Allen JC, Boettcher AL (1978) Amphiboles in andesite and basalt: II. Stability as a function of $P-T-f_{H_2O}-f_{O_2}$. Am Mineral 63:1074–1087

Anderson AT (1976) Magma mixing: Petrological process and volcanological tool. J Volcan Geotherm Res 1:3–33

Anderson AT (1968) The oxygen fugacity of alkaline basalt and related magmas, Tristan Da Cunha. Am J Sci 266:704–727

Anderson AT, Wright TL (1972) Phenocryst and glass inclusions and their bearing on oxidation and mixing of basaltic magmas, Kilauea volcano, Hawaii. Am Mineral 57:188–216

Ando S (1975) Minor element geochemistry of the rocks from Mashu Volcano, Eastern Hokkaido. J Fac Sci Hokkaido Univ Ser 4, 16:553–566

Armstrong RL, Cooper JA (1971) Lead isotopes in Island Arcs. Bull Volcanol XXXV-1:27–63

Arth JG (1976) Behavior of trace elements during magmatic processes: A summary of theoretical models and their application. J Res US Geol Surv 4:41–47

Bibee LD, Shor GG Jr, Lu RS (1980) Inter-arc basin spreading in the Mariana Trough. Mar Geol 35:183–197

Boettcher AL (1977) The role of amphiboles and water in circumpacific volcanism. High pressure research, applications in geophysics, Manghnani MH et al. (eds), Academic Press Inc New York, pp 107–125

Carmichael ISE, Nichols J (1967) Iron-titanium oxides and oxygen fugacities in volcanic rocks. J Geophys 72:4665–4687

Carr MJ (1976) Underthrusting and quaternary faulting in northern Central America. Bull Geol Soc Am 87:825–829

Cawthorn RG, O'Hara MJ (1976) Amphibole Fractionation in calc-alkaline magma genesis. Am J Sci 276:309–329

Church SE (1976) The Cascade Mountains Revisited: A re-evaluation in light of new lead isotope data. Earth Planet Sci Lett 29:175–188

Cloud PE Jr, Schmidt RG, Burke HW (1956) Geology of Saipan, Mariana Islands. US Geol Surv Prof Pap 280-A; 126 pp

Condie KC, Swenson DH (1973) Compositional variation in three Cascade stratovolcanoes: Jefferson, Rainier, and Shasta. Bull Volcanol 37:205–230

DePaulo DJ, Wasserburg GJ (1977) The sources of island arcs as indicated by Nd and Sr isotopic studies. Geophys Res Lett 4: 465–468

DePaulo DJ, Johnson RW (1979) Magma genesis in the New Britain island arc: Constraints from Nd and Sr isotopes and trace element patterns. Contrib Mineral Petrol 70:367–379

Dixon TH, Batiza R (1979) Petrology and chemistry of recent lavas in the Northern Marianas: Implications for the origin of Island Arc Basalts. Contrib Mineral Petrol 70:167–181

Dungan MA, Rhodes JM (1978) Residual glasses and melt inclusions in basalts from DSDP. Legs 45 and 46: Evidence for magma mixing. Contrib Mineral Petrol 67:417–431

Eggler DH (1972) Amphibole stability in H_2O-undersaturated calc-alkaline melts. Earth Planet Sci Lett 15:28–34

Eggler DH, Burnham CW (1973) Crystallization and fractionation trends in the system andesite – $H_2O-CO_2-O_2$ at pressures to 10 Kb. Bull Geol Soc Am 84:2517–2532

Ewart A, Stipp JJ (1968) Petrogenesis of the volcanic rocks of the Central North Island, New Zealand, as indicated by a study of Sr^{87}/Sr^{86} ratios and Sr, Rb, K, U and Th abundances. Geochim Cosmochim Acta 32:699–736

Ewart A (1976) Mineralogy and chemistry of modern orogenic lavas – Some statistics and implications. Earth Planet Sci Lett 31:417–432

Fudali RF (1965) Oxygen fugacities of basaltic and andesitic magmas. Geochim Cosmochim Acta 29:1063–1075
Garcia MO, Jacobson SS (1979) Crystal clots, amphibole fractionation, and the evolution of calc-alkaline magmas. Contrib Mineral Petrol 69:319–332
Gill JB (1978) Role of trace element partition coefficients in models of andesite genesis. Geochim Cosmochim Acta 42:709–724
Hawkesworth CJ, O'Nions RK, Arculus RJ (1979) Nd and Sr isotope geochemistry and island arc volcanics, Grenada, Lesser Antilles. Earth Planet Sci Lett 45:237–248
Helz RT (1976) Phase relations of basalts in their melting ranges at P_{H_2O}=SKb. Part II. Melt compositions. J Petrol 17:139–193
Hibbard MJ (1981) The magma mixing origin of mantled feldspars. Contrib Mineral Petrol 76:158–170
Holloway JR, Burnham CW (1972) Melting relations of basalt with equilibrium water pressure less than total pressure. J Petrol 13:1–29
Hussong DM, Uyeda S, et al. (1981) Initial Reports of the Deep Sea Drilling Project 60, Washington, US Govern Printing Office
Irvine TN, Baragar WRA (1971) A guide to the chemical classification of the common volcanic rocks. Can J Earth Sci 8:523–548
Jacobs JW, Korotev RL, Blanchard DP, Haskin LA (1977) A well-tested procedure for instrumental neutron-activation analysis of silicate rocks and minerals. J Radioanal Chem 40:93–114
Karig DE (1971) Structural history of the Mariana Island arc system. Bull Geol Soc Am 42:323–344
Katsui Y, Ando S, Inaba K (1975) Formation and magmatic evolution of Mashu Volcano, East Hokkaido, Japan. J Fac Sci Hokkaido Univ Ser 4, 16:533–552
Katsumata M, Sykes LR (1969) Seismicity and tectonics of the Western Pacific: Izu-Mariana-Caroline and Ryukyu-Taiwan regions. J Geophys Res 74:5923–5948
Kay WR, Sun SS, Lee-Hu CN (1978) Pb and Sr isotopes in volcanic rocks from the Aleutian Islands and Pribilof Islands, Alaska. Geochim Cosmochim Acta 42:263–273
Kuno H (1950) Petrology of Hakone Volcano and the adjacent areas, Japan. Bull Geol Soc Am 61:957–1020
Kuno H (1962) Catalogue of the active volcanoes of the world including solfatara fields: Part II, Japan, Taiwan, and Marianas. Int Assoc Volcanol 1–332
Larson RL, Chase CG (1972) Late Mesozoic evolution of the Western Pacific Ocean. Geol Soc Am Bull 83:3627–3644
La Traille SL, Hussong DM (1980) Crustal structure across the Mariana island arc. in The Tectonic evolution of Southeast Asian Seas and Islands: DE Hayes (ed). Am Geophys Union Monogr 23:209–221
Luhr JF, Carmichael ISE (1980) The Colima Volcanic Complex, Mexico. Contrib Mineral Petrol 71:343–372
Marsh BD (1979) Island arc development: Some observations, experiments, and speculations. J Geol 87:p 687
Meijer A (1976) Pb and Sr isotopic data bearing on the origin of volcanic rocks from the Mariana island-arc system. Bull Geol Soc Am 87:1358–1369
Meijer A, Anthony E, Reagan M (1981) Petrology of volcanic rocks from the fore-arc sites. In: Hussong D, Uyeda S, et al. (eds) Initial reports of the Deep Sea Drilling Project 60
Meijer A (1981) Regional distribution and character of active andesite volcanism (f) Mariana-volcano islands. In: RS Thorpe (ed) Orogenic andesites and related rocks, Wiley and Sons, New York
Miyashiro A (1974) Volcanic rock series in island arcs and active continental margins. Am J Sci 274:321–355
Mueller RF, Saxena SK (1977) Chemical petrology with applications to the terrestrial planets and meteorites. Springer-Verlag, New York, 394 pp
Nelson SA (1980) Geology and petrology of Volcan Ceboruco, Nayarit, Mexico – Summary. Geol Soc Am Bull 91:p 639
Osborn EF (1959) Role of oxygen pressure in the crystallization and differentiation of basaltic magma. Am J Sci 257:609–647
Osborn EF (1962) Reaction series for subalkaline igneous rocks based on different oxygen pressure conditions. Am Mineral 47:211–216
Osborn EF (1976) Origin of calc-alkali magma series of santorini volcano type in the light of recent experimental phase equilibrium studies. In: Proceedings of the International Crongress on thermal waters, geothermal energy and volcanism of the Mediterranean area, Athens, Greece, October 1976, 3:154–167
Oversby VM, Ewart A (1972) Lead isotopic compositions of Tonga-Kermadec volcanics and their petrogenetic significance. Contrib Mineral Petrol 37:181–210
Pearce JA, Norry MJ (1979) Petrogenetic implications of Ti, Zr, Y, and Nb variation in volcanic rocks. Contrib Mineral Petrol 69:33–47
Philpotts JA, Schnetzler CC (1970) Phenocryst – matrix partition coefficients for K, Rb, Sr, and Ba, with applications to anothorite and basalt genesis. Geochim Cosmochim Acta 36:1131–1166
Powell M (1978) Crystallization conditions of low-pressure cumulate nodules from the Lesser Antilles Island arc. Earth Sci Lett 39:162–172
Presnall DC (1966) The join forsterite-diopside-iron oxide and its bearing on the crytallization of basaltic and ultramafic magmas. Am J Sci 264:753–809
Ringwood AE (1974) The petrological evolution of island arc systems. J Geol Soc Land 130:183–204
Ritchey JL (1980) Divergent magmas at Crater Lake, Oregon: Products of fractional crystallization and vertical zoning in a shallow, water-undersaturated chamber. J Volcanol Geotherm Res 7:373–386
Ritchey JL, Eggler DH (1978) Amphibole stability in a differentiated calc-alkaline magma chamber: An experimental investigation. In: Annual Report of the Director, Geophysical Laboratory. Carnegie Inst Washington Yearb 77:790–793
Roeder PL, Osborn EF (1966) Experimental data for the system $MgO-FeO-Fe_2O_3-CaAl_2Si_2O_8-SiO_2$ and their petrogenetic implications. Am J Sci 264:753–809
Rose WI Jr, Grant NK, Hahn GA, Lange IM, Powell JL, Easter J, Degraff JM (1977) The evolution of Santa Maria Volcano, Guatemala. J Geol 85:63–87
Sato H (1977) Nickel content of basaltic magmas: Identification of primary magmas and a measure of the degree of olivine fractionation. Lithos 10:113–120
Seno T (1977) The instantaneous rotation vector of the Philippine sea plate relative to the Eurasian plate. Tectonophysics 42:209–226
Sharp ADL, Davis PM, Gray F (1980) A low velocity zone beneath Mount Etna and magma storage. Nature 287:587–591
Sinha AK, Hart SR (1972) A geochemical test of the subduction hypothesis for generation of island arc magmas. Carnegie Inst Washington Yearb 71:309–312
Stern RJ, Bibee LD (1980) Esmeralda Bank: The structure and geochemistry of an active submarine volcano in the Mariana Island arc. Geol Soc Am (Abstr with Progr) 12
Stewart DC (1975) Crystal clots in calc-alkaline andesites as breakdown products of high-Al amphiboles. Contrib Mineral Petrol 53:1975–204
Tracey JI Jr, Schlanger SO, Stark JT, Doan DB, May HG (1963) General geology of Guam. US Geol Surv Prof Pap 403-A; 104 pp
Turner JS (1980) A fluid-dynamical model of differentiation and layering in magma chambers. Nature 285:213–215 (1980)
Wells PRA (1977) Pyroxene thermometry in simple and complex systems. Contrib Mineral Petrol 62:129–139
Wood BJ, Banno S (1973) Garnet-orthopyroxene and orthopyroxene-clinopyroxene relationships in simple and complex systems. Contrib Mineral Petrol 42:109–124
Woodruff LG, Rose WI Jr, Rigot W (1979) Contrasting fractionation patterns for sequential magmas from two calc-alkaline volcanoes in Central America. J Volcanol Geotherm Res 6:217–240
Wright TL, Doherty PC (1970) A linear programming and lease squares computer method for solving petrologic mixing problems. Geol Soc Am Bull 81:1995–2008
Yoder HS Jr (1969) Calc-alkaline andesites: Experimental data bearing on the origin of their assumed characteristics: Proceedings of the Andesite Conference. Oreg, Dep Geol Miner Ind, Bull 65:77–89

Received March 28, 1981; Accepted in revised form September 18, 1981